

# Rational design of phytovirucide inhibiting nucleocapsid protein aggregation in tomato spotted wilt virus

Received: 29 May 2024

Accepted: 17 February 2025

Published online: 27 February 2025

Ningning Zan , Jiao Li , Jiahui Yao , Shang Wu , Jianzhan Li , Feifei Chen, Baoan Song  & Runjiang Song 

Ineffectiveness of managing plant viruses by chemicals has posed serious challenges in crop production. Recently, phase separation has shown to play a key role in viral lifecycle. Using inhibitors that can disturb biomolecular condensates formed by phase separation for virus control has been reported in medical field. However, the applicability of this promising antiviral tactic for plant protection has not been explored. Here, we report an inhibitor, **Z9**, that targets the tomato spotted wilt virus (TSWV) N protein. **Z9** is capable of interacting with the amino acids in the nucleic acid binding region of TSWV N, disrupting the assembly of N and RNA into phase-separated condensates, the reduction of which is detrimental to the stability of the N protein. This study provides a strategy for phase separation-based plant virus control.

Biomolecular condensates are related to many cellular processes, including the compartmentalization of biochemical reactions, the sensing and response to stress, mechanical regulation, and signal transduction<sup>1,2</sup>. Increasing evidence suggests that phase separation is a fundamental principle for the formation of biomolecular condensates<sup>3–6</sup>. The assembly components of condensates are typically complex and usually involve proteins and nucleic acids, which lead to phase separation via their multivalent interactions<sup>7–10</sup>. As obligate intracellular parasites, viruses rely on cellular functions and processes to enable efficient replication. During infection, condensate-like structures commonly referred to as replication compartments (RCs) or inclusion bodies (IBs) are formed by viral proteins. Importantly, recent studies have implicated phase separation as a driving force for the formation of these biomolecular condensates<sup>11,12</sup>. The condensates play key roles in viral life cycles, including viral entry<sup>13</sup>, genome synthesis and replication<sup>14</sup>, assembly of new particles<sup>15</sup>, and escape from antiviral defense pathways<sup>16</sup>.

Condensates formed by phase separation have attracted much attention in the pharmaceutical industry and academia as novel targets in drug discovery<sup>17–19</sup>. Although some small molecules have been shown to regulate the aggregation of viral biomolecular condensates in recent years, the discovery of new structures is still relatively rare<sup>20–23</sup>. Moreover, such modulators have not been reported in the

agricultural field. Replication-related proteins encoded by several plant viruses, such as barley yellow striate mosaic virus (BYSMV), tomato yellow mottle-associated virus (TYMaV), tomato bushy stunt virus (TBSV), and carnation Italian ringspot virus (CIRV), have all been found to form condensates, which have been associated with phase separation in the past two years<sup>24–26</sup>. Recently, phytochemical type III effectors have been shown to exhibit a propensity for phase separation<sup>27</sup>. Thus, targeting biomolecular condensates may be promising for the successful development of pesticides for treating plant diseases that are difficult to control. Tomato spotted wilt virus (TSWV) belongs to the family *Tospoviridae* and is one of the most devastating plant viruses worldwide, causing an annual economic loss of over one billion US dollars<sup>28</sup>. The use of antiviral agents can effectively slow down the occurrence and spread of viral diseases, making it one of the effective control strategies. But currently, commercialized drugs cannot actually serve the purpose of managing TSWV-induced disease<sup>29</sup>. Therefore, developing an effective anti-TSWV agents is highly important. The few proteins encoded by the TSWV genome play important roles in virus infection. Among them, the nucleocapsid protein (N) is an important component of the core template ribonucleoprotein (RNP) for viral replication<sup>30</sup> and has multiple biological functions in the viral life cycle. The genomic RNA of viruses can be well protected in RNPs against RISC-mediated cleavage<sup>31</sup>. Similar to animal-infecting

*Bunyaviruses*<sup>32</sup>, TSWV relies on a cap-snatching mechanism to initiate transcription of its genome<sup>33</sup>. The N proteins partially colocalize with processing bodies (PBs) and stress granules (SGs), which are the sources of 5' capped RNA<sup>34</sup>. Notably, the N protein is capable of forming highly motile cytoplasmic IBs that traffic on actin filaments<sup>35</sup>. Therefore, the N protein can serve as an important molecular target for the creation of anti-TSWV agents.

Chromones are an important class of natural active ingredients produced during secondary metabolism in plants. Their structure is easy to modify and is considered a good lead skeleton for drug discovery<sup>36</sup>. Chromone compounds derived from natural products have potential broad-spectrum antiviral effects against human viruses, including severe acute respiratory syndrome coronavirus 2 (SARS-CoV-2), herpes simplex virus type 1 (HSV1), influenza A virus (IAV), and hepatitis B virus (HBV)<sup>37,38</sup>. We previously synthesized several types of chromone compounds that possess good inhibitory activity against plant viruses and found that they have good binding ability to coat proteins (Fig. 1a)<sup>29,39</sup>. Dithiocarbamates (DTCs) serve as a broad-spectrum pharmacophore widely present in marketed drugs across the medical and agricultural fields<sup>40</sup>. By integrating DTC with various bioactive scaffolds, the compounds' interaction with targets can be enhanced, thereby significantly boosting their biological activity<sup>41–43</sup>. Cationic amphiphilic drugs (CADs) are a class of commercialized drugs with a wide range of medical activities<sup>44</sup>. They are characterized by a common structure, namely, hydrophobic aromatic side chains containing an amine functional group, which is crucial for their pharmacological activity by increasing the pH in acidic intracellular compartments<sup>45</sup>. The phase separation modulators obtained through high-throughput screening methods appear to possess the properties of CADs (Fig. 1b)<sup>46–50</sup>. Notably, an increasing number of studies emphasize the crucial role of pH in the formation of condensates<sup>51–54</sup>. Therefore, we propose that designing a compound with CAD properties may be more successful in discovering a biomolecular condensate modulator.

In this work, we design a series of chromone compounds containing hydrophilic amine groups with piperazine dithiocarbamate as the bond bridge and obtain the target compounds in high yields (Fig. 1c). We find that the introduction of tertiary amine groups significantly enhances the anti-TSWV activities of these compounds. The highly active compound **Z9** can target the N protein to inhibit the replication level of the viral ribonucleoprotein (RNP), thereby affecting virus proliferation in vivo. Application of **Z9** can lead to a decrease in N protein condensation in plant cells. Furthermore, **Z9** acts on condensates with phase separation properties, not on large solid-like granules. Interestingly, the reduction in the number of N condensates affects the stability of the N protein in plants. Moreover, we demonstrate that key sites or the addition of **Z9** significantly affect the ability of the N protein to bind with RNA to form condensates. Overall, this study points to an important direction for pesticide discovery and crop virus control.

## Results

### Anti-TSWV activity

The inhibitory activities of the target compounds **Z1–Z25** against TSWV were assessed via the half-leaf method, with *Nicotiana glutinosa* serving as the model plant. Preliminary screening at a concentration of 500 µg/mL revealed that the curative activity range of compounds **Z1–Z25** against TSWV ranged from 43.5% to 64.4%, protective activities varied between 43.1% and 65.4%, and inactivation activities from 41.4% to 77.3%. Among them, compounds **Z9** (77.3%), **Z13** (72.8%), **Z14** (70.6%), and **Z17** (74.2%) had excellent inactivation activity against TSWV, outperforming the control ningnanmycin (69.3%), and were significantly superior to ribavirin (43.7%). We found that the inhibitory activities of compounds (**Z1–Z7**) without tertiary amine groups on TSWV were average. The EC<sub>50</sub> values of the compounds were further

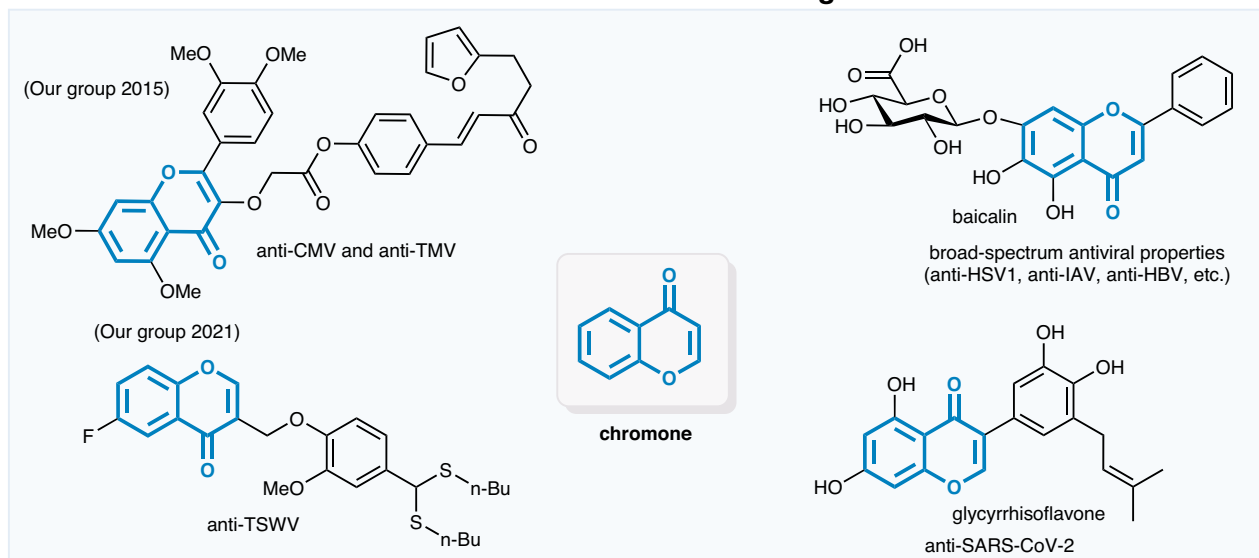
tested, and the results revealed that compound **Z9** exhibited the best inactivation activity against TSWV, with inhibitory activity of 65.3 µg/mL, which was significantly better than that of the best anti-plant viral agent currently available on the market, ningnanmycin (149.4 µg/mL), and another commonly used antiviral agent, ribavirin (801.5 µg/mL) (Table 1). The above results indicate that the introduction of a tertiary amine substantially enhances the anti-TSWV activities of these compounds.

Furthermore, the inhibitory effect of compound **Z9** on TSWV was validated in tomatoes in addition to model plants. The tomato plants sprayed with 3% Tween 80 presented severe symptoms, including curled leaves, dark brown spots, delayed development, and yellowing. In contrast, plants treated with compound **Z9** showed a significant alleviation in symptom severity, with improved growth and larger, greener leaves compared to untreated controls (Fig. 2a). These findings could indicate that compound **Z9** significantly reduces the proliferation of TSWV in plants. The broad-spectrum antiviral activity of compound **Z9** was further evaluated against a panel of plant viruses, and the results revealed that the inhibition rates of compound **Z9** at 500 µg/mL against CMV, PVY, PMMoV, and TMV were 76.6%, 73.4%, 70.8%, and 79.0%, respectively. These rates are comparable to those of ningnanmycin (74.2%, *t*-test, *P* = 0.5168; 77.6%, *t*-test, *P* = 0.0422; 72.0%, *t*-test, *P* = 0.6586; and 83.1%, *t* test, *P* = 0.2275) and significantly better than those of ribavirin (52.4%, *t*-test, *P* = 0.0013; 55.3%, *t*-test, *P* = 0.0059; 56.5%, *t* test, *P* = 0.0049; and 54.0%, *t* test, *P* = 0.0036) (Supplementary Fig. 1a–h). This result indicates that **Z9** is a compound with broad-spectrum antiviral activity against plant viruses.

### Compound **Z9** inhibits normal replication of RNPs by targeting the N protein

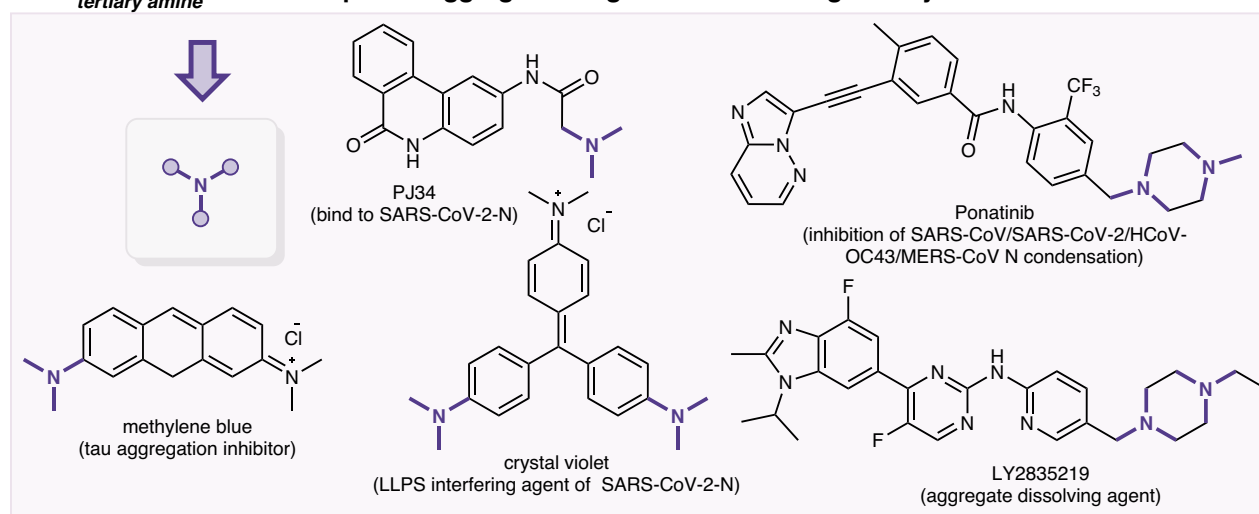
The ribonucleoprotein complex (RNP) of TSWV is responsible for executing the transcription and replication of the viral genome, playing a crucial role in the viral lifecycle<sup>28,30,31</sup>. The competent minigenome replication system (L<sub>(+)</sub>opt<sup>+</sup> SR<sub>(+)</sub>eGFP + VSRs) (Fig. 2b) can be used to study the replication levels of reconstituted RNP<sup>55</sup>. To investigate the mode of action of compound **Z9**, a replication system was used to detect the effect of compound **Z9** on the replication of RNP in *Nicotiana benthamiana*. We observed that the fluorescence levels in the infiltrated leaves, monitored 5 days post-application of compound **Z9**, were significantly lower than those in the untreated leaves, as determined by fluorescence microscopy (Fig. 2c). Western blot analysis further revealed that the accumulation levels of N protein in infiltrating leaves were consistent and considerably decreased relative to those in the untreated leaves (Fig. 2d). These findings indicate that compound **Z9** effectively inhibits the replication of the RNP of TSWV in plants. The N protein, on the other hand, serves as the main assembly protein of the viral RNP<sup>28,30,31</sup> and was explored as a potential target for these compounds. To assess this, His-tagged N protein was fixed to the sensor (Ni-NTA), and compounds with different inhibitory activities were used for rapid detection of binding signal values (Fig. 2e). The results of the bio-layer interferometry (BLI) assay revealed that compounds with poor activity presented weak binding signals, essentially below 0.10 nm. Conversely, compounds with potent activity presented higher binding signal values with the N protein (Fig. 2f), although a consistently strong positive correlation between activity and signal values was not apparent for every compound. For example, compounds **Z1** and **Z8** presented lower binding signal values than compounds **Z2** and **Z12** did. The introduction of amine groups greatly improved the binding of the compounds to the N protein. The binding signal between compound **Z9** and the N protein was the highest, with an affinity constant of 7.6 µM (Fig. 2g). These findings suggest that the N protein may serve as a target for this class of compounds. In addition, this method is beneficial for rapid screening of small molecules that target N proteins in vitro. To

## a. Chromone and its antiviral analogues



skeleton of tertiary amine

## b. Reported aggregation regulators containing tertiary amines



## c. This work

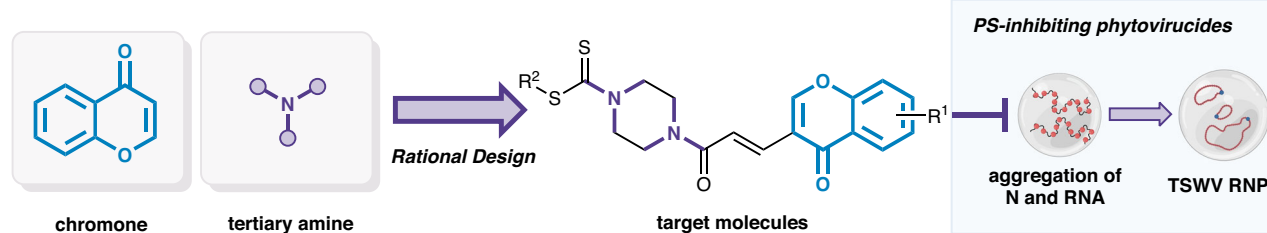


**Fig. 1 | Design strategy for biomolecular condensate-inhibiting phytovirucides.** **a** The structures of chromone and its antiviral analogs. **b** The structures of reported aggregation regulators containing tertiary amines. **c** Rational design of phase-separated (PS) condensates-inhibiting phytovirucides in the study.

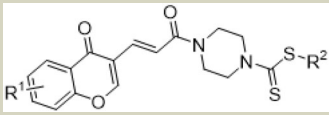
confirm that the N protein is a direct target of compound **Z9**, a probe was synthesized by introducing an alkyne group into the side chain of compound **Z9** (Supplementary Fig. 2a, b). The results of the activity assay indicated that the probe possessed good inhibitory activity against TSWV (Supplementary Table 1). The competitive binding experiment result showed that the probe and compound **Z9** had the same binding region for the N protein (Supplementary Fig. 2c). We found that the protein labeled by the probe in the total protein of healthy leaves and diseased leaves seem to be similar. However, pull-down assays clearly demonstrated that the probe significantly captured the N protein from diseased leaf extracts

(Supplementary Fig. 2d). These results provide direct evidence that the N protein is a target of compound **Z9**.

### Compound **Z9** significantly reduces N protein condensates

The TSWV N protein can form motile cytoplasmic IBs to promote the proliferation of viruses<sup>33–35</sup>. We aimed to observe the impact of compound **Z9** on the behavior of N protein condensates in vivo. N-YFP was transiently expressed in *N. benthamiana* leaves, and after 18 h, the diluted phase of N-YFP was clearly visible. Compound **Z9** or DMSO was injected into the left side of the same infiltrated leaves, and the formation of IBs was monitored at 36 and 72 h post-injection

**Table 1 | Anti-TSWV activity assay in vivo**

Compound			Curative effect (%)	Protective effect (%)	Inactive effect (%)	EC <sub>50</sub> (μg/mL)
	R <sup>1</sup>	R <sup>2</sup>				
<b>Z1</b>	H	CH <sub>2</sub> CH <sub>3</sub>	56.3 ± 7.9	52.5 ± 5.6	54.1 ± 4.3	354.8 ± 11.5
<b>Z2</b>	H	(CH <sub>2</sub> ) <sub>2</sub> CH <sub>3</sub>	53.4 ± 9.0	48.7 ± 7.4	48.5 ± 3.2	595.0 ± 13.9
<b>Z3</b>	H	(CH <sub>2</sub> ) <sub>3</sub> CH <sub>3</sub>	46.8 ± 7.2	43.3 ± 2.1	54.8 ± 6.4	430.2 ± 7.9
<b>Z4</b>	H	CH <sub>2</sub> CH(CH <sub>3</sub> ) <sub>2</sub>	48.3 ± 3.5	49.8 ± 5.3	50.7 ± 7.5	487.2 ± 9.2
<b>Z5</b>	H	(CH <sub>2</sub> ) <sub>4</sub> CH <sub>3</sub>	43.5 ± 5.7	43.1 ± 2.7	41.4 ± 4.6	598.6 ± 8.2
<b>Z6</b>	H	Cyclopropyl	47.4 ± 3.6	54.9 ± 3.4	55.7 ± 2.5	358.5 ± 7.6
<b>Z7</b>	H	CH <sub>2</sub> Ph	51.9 ± 2.3	47.2 ± 5.8	53.2 ± 5.4	433.5 ± 9.3
<b>Z8</b>	H	(CH <sub>2</sub> ) <sub>2</sub> N(CH <sub>3</sub> ) <sub>2</sub>	62.1 ± 2.5	60.8 ± 3.9	71.6 ± 7.9	132.7 ± 8.6
<b>Z9</b>	H	(CH <sub>2</sub> ) <sub>3</sub> N(CH <sub>3</sub> ) <sub>2</sub>	64.4 ± 7.9	65.3 ± 2.4	77.3 ± 3.7	65.3 ± 7.2
<b>Z10</b>	H	(CH <sub>2</sub> ) <sub>2</sub> N(CH <sub>2</sub> CH <sub>3</sub> ) <sub>2</sub>	57.2 ± 1.8	59.5 ± 4.9	62.2 ± 1.9	235.4 ± 8.1
<b>Z11</b>	H	(CH <sub>2</sub> ) <sub>3</sub> N(CH <sub>2</sub> CH <sub>3</sub> ) <sub>2</sub>	61.5 ± 3.7	58.7 ± 5.4	63.1 ± 4.3	183.5 ± 7.5
<b>Z12</b>	6-F	(CH <sub>2</sub> ) <sub>2</sub> N(CH <sub>3</sub> ) <sub>2</sub>	64.2 ± 6.1	64.3 ± 4.3	69.5 ± 5.6	137.6 ± 6.9
<b>Z13</b>	6-F	(CH <sub>2</sub> ) <sub>3</sub> N(CH <sub>3</sub> ) <sub>2</sub>	60.7 ± 3.5	63.8 ± 7.2	72.8 ± 3.5	125.8 ± 9.2
<b>Z14</b>	6-F	(CH <sub>2</sub> ) <sub>2</sub> N(CH <sub>2</sub> CH <sub>3</sub> ) <sub>2</sub>	63.3 ± 6.9	65.4 ± 6.4	70.6 ± 3.8	103.6 ± 8.4
<b>Z15</b>	6-F	(CH <sub>2</sub> ) <sub>3</sub> N(CH <sub>2</sub> CH <sub>3</sub> ) <sub>2</sub>	58.0 ± 5.6	61.5 ± 4.2	62.4 ± 2.6	164.2 ± 9.5
<b>Z16</b>	6-OCH <sub>3</sub>	(CH <sub>2</sub> ) <sub>2</sub> N(CH <sub>3</sub> ) <sub>2</sub>	60.7 ± 3.0	59.4 ± 2.1	63.7 ± 3.9	127.5 ± 8.3
<b>Z17</b>	6-OCH <sub>3</sub>	(CH <sub>2</sub> ) <sub>3</sub> N(CH <sub>3</sub> ) <sub>2</sub>	62.5 ± 7.4	64.7 ± 2.5	74.2 ± 6.3	78.5 ± 6.7
<b>Z18</b>	6-OCH <sub>3</sub>	(CH <sub>2</sub> ) <sub>2</sub> N(CH <sub>2</sub> CH <sub>3</sub> ) <sub>2</sub>	58.5 ± 1.6	60.2 ± 8.7	59.7 ± 7.2	162.4 ± 9.7
<b>Z19</b>	6-OCH <sub>3</sub>	(CH <sub>2</sub> ) <sub>3</sub> N(CH <sub>2</sub> CH <sub>3</sub> ) <sub>2</sub>	59.6 ± 3.8	57.5 ± 5.6	60.1 ± 5.9	154.3 ± 9.6
<b>Z20</b>	7-F	(CH <sub>2</sub> ) <sub>2</sub> N(CH <sub>3</sub> ) <sub>2</sub>	60.3 ± 6.7	62.7 ± 3.5	65.6 ± 3.5	118.7 ± 6.4
<b>Z21</b>	7-F	(CH <sub>2</sub> ) <sub>3</sub> N(CH <sub>3</sub> ) <sub>2</sub>	62.7 ± 3.8	63.4 ± 4.1	67.3 ± 7.4	109.5 ± 7.5
<b>Z22</b>	7-F	(CH <sub>2</sub> ) <sub>2</sub> N(CH <sub>2</sub> CH <sub>3</sub> ) <sub>2</sub>	60.6 ± 2.6	58.8 ± 6.3	57.5 ± 6.7	252.8 ± 8.9
<b>Z23</b>	7-F	(CH <sub>2</sub> ) <sub>3</sub> N(CH <sub>2</sub> CH <sub>3</sub> ) <sub>2</sub>	56.2 ± 6.1	54.5 ± 2.8	58.2 ± 5.3	235.7 ± 8.5
<b>Z24</b>	7-OCH <sub>3</sub>	(CH <sub>2</sub> ) <sub>2</sub> N(CH <sub>3</sub> ) <sub>2</sub>	57.4 ± 5.5	55.6 ± 3.7	61.9 ± 2.5	178.6 ± 7.4
<b>Z25</b>	7-OCH <sub>3</sub>	(CH <sub>2</sub> ) <sub>2</sub> N(CH <sub>2</sub> CH <sub>3</sub> ) <sub>2</sub>	56.5 ± 3.9	53.7 ± 2.3	57.2 ± 4.6	287.4 ± 8.2
Ningnanmycin			57.9 ± 1.5	61.7 ± 5.2	69.3 ± 2.4	149.4 ± 8.7
Ribavirin			39.2 ± 3.2	40.4 ± 6.8	43.7 ± 7.5	801.5 ± 12.6

Note: Data are presented as mean ± standard deviation. *n* = 3. Ningnanmycin and ribavirin were used as the positive control.

via z-stack scanning (Fig. 3a). Compared with DMSO, compound **Z9**, at a concentration of 100 μg/mL, significantly reduced the number of small IBs or their diffuse distribution in the leaf cell infiltration area at 36 h, and the number of IBs in the leaves treated with compound **Z9** was reduced by more than half at 72 h (*t*-test, *P* = 0.0001) (Fig. 3b, c). The accumulation levels of the N-YFP protein were further detected. The results indicated a significant reduction in the accumulation level of the N-YFP protein following the addition of compound **Z9** (Fig. 3d). In *N. benthamiana* cells, highly motile cytoplasmic IBs formed by N-YFP can be clearly observed at 36 h (Supplementary Movie 1). To explore whether compound **Z9** has an elimination effect on small particles, N-YFP was transiently expressed in *N. benthamiana* leaves, and after 36 h, drugs were injected into the infiltration area, and the IBs 5 h post-injection were observed (Supplementary Fig. 3a). Compound **Z9**, at a concentration of 100 μg/mL, significantly reduced the number of IBs in the leaf cell infiltration area (*t* test, *P* = 0.0001), whereas compound **Z3**, with less effective anti-TSWV activity, had a relatively weaker ability to disperse the condensates (*t*-test, *P* = 0.0075) (Supplementary Fig. 3b–d). The above results revealed that compound **Z9**, with an amine group, could effectively inhibit the formation of aggregates involving the N protein.

Although several types of anti-TSWV compounds targeting N proteins have been previously reported, their impact on IBs has not been explored<sup>29,56,57</sup>. Herein, we further investigated whether other

highly active compounds similar to CADs can disrupt the aggregation of the N protein. Piperazine derivatives containing ethyl morpholine indeed inhibited IB formation (Supplementary Fig. 3e, f). Further extraction and transformation of *N. benthamiana* protoplasts revealed that N-eGFP formed condensates within the cells, and within 30 min, larger N-eGFP particles remained condensed in intact cells after treatment with compound **Z9** at a concentration of 10 μg/mL, whereas smaller N-eGFP particles disappeared in intact cells (Fig. 3e). Therefore, the above experimental results reveal the potential mechanism by which drugs targeting the N protein may act by degrading small condensates. Although compound **Z9** could act on plant proteins, we found that **Z9** had not any adverse effects on the growth and development of plants (Supplementary Fig. 4a). To investigate whether compound **Z9** have the same effects of on the other viral proteins, the binding capabilities of compound **Z9** with PVY CP and PMMoV CP were first tested. The results showed that the binding constants of compound **Z9** with these two proteins were 67 μM and 18 μM, respectively (Supplementary Fig. 4b–d), indicating a good binding capability between compound **Z9** and PMMoV CP. Thus, PMMoV CP in leaves was treated using the same method. Through fluorescence observation, we found that PMMoV CP did not significantly decrease at 5 h and 18 h after compound **Z9** treatment (Supplementary Fig. 4e, f), while compound **Z9** could significantly reduce the number of TSWV N protein condensates in cells. This seems to suggest that **Z9** is more easily



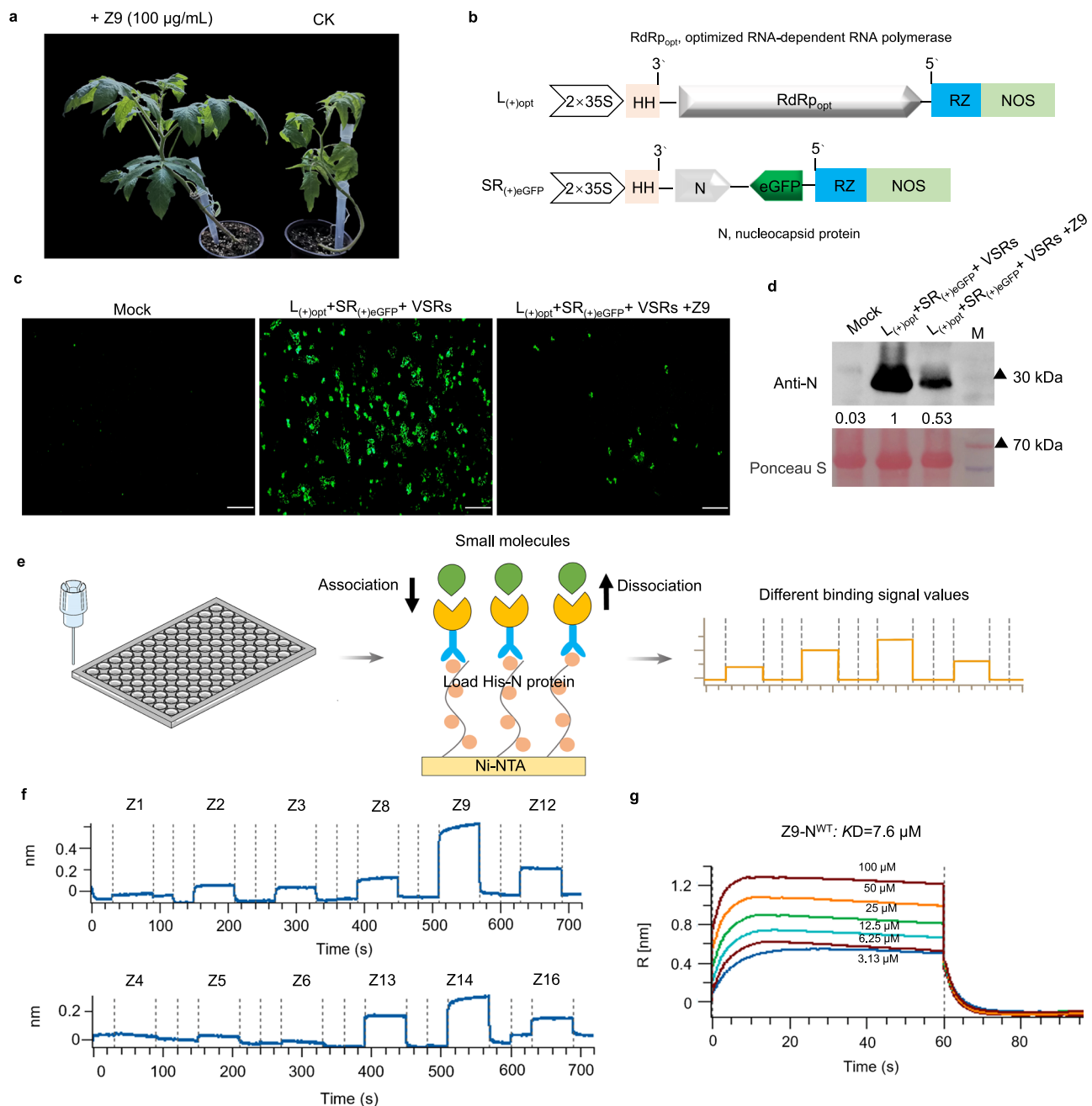


**Fig. 2 | Action mode of compound Z9 inhibiting TSWV. a** Compound Z9 could inhibit the proliferation of TSWV in tomatoes from the appearance of symptoms. **b** Schematic diagrams of the constructs SR(+)<sub>eGFP</sub> and L(+)<sub>opt</sub>. L(+)<sub>opt</sub>, a full-length infectious clone of TSWV L genomic RNA fragment with optimized RNA-dependent RNA polymerase (RdRp<sub>opt</sub>); SR(+)<sub>eGFP</sub>, an infectious clone of TSWV S genomic RNA with nucleocapsid protein (N), in which NSs of TSWV S genome RNA fragment is replaced by eGFP. Plus sign (+) and 3' to 5' designation indicate the antigenomic RNA of TSWV; 2×35S, a double 35S promoter; HH, hammerhead ribozyme; RZ, hepatitis delta virus (HDV) ribozyme; NOS, nopaline synthase terminator. **c** The amounts of fluorescence in the infiltrated leaves were observed at the 5<sup>th</sup> day. Bars,

500 µm. The experiment was repeated three times showing similar results. **d** Western blot was used to detect the accumulation level of protein N in the infiltrated leaves. Staining of RuBisCO with Ponceau S was used as a sample loading control. The experiment was repeated three times showing similar results. **e** Pattern diagram of continuous detection of binding signal values between small molecules and N protein using BLI. **f** The binding signal values between compounds with different activities and N protein. Compounds Z1–Z6 are compounds with average activities, while compounds Z8, Z9, Z12, Z13, Z14, and Z16 are compounds with good activity. **g** The binding ability of compound Z9 with wild-type N protein (N<sup>WT</sup>) was measured by BLI. Source data are provided as a Source Data file.

recruited to condensates rather than dilute phases and Z9 has a unique mechanism of action against TSWV.

### N protein condensates in vivo possess phase separation properties

We further delved into the mechanism behind the reduction in the number of condensates observed upon the addition of compound Z9.

Within cells, proteins and nucleic acids, which are biological macromolecules, can undergo a process known as phase separation to form membraneless organelles<sup>3–6</sup>. With this premise, the phase separation potential of the N protein was assessed using the Predictor of Natural Disordered Regions (PONDR) VL-XT algorithm. This sequence-based prediction is based on the IDR of the N protein, which is located primarily within its central core domain (Supplementary Fig. 5a).

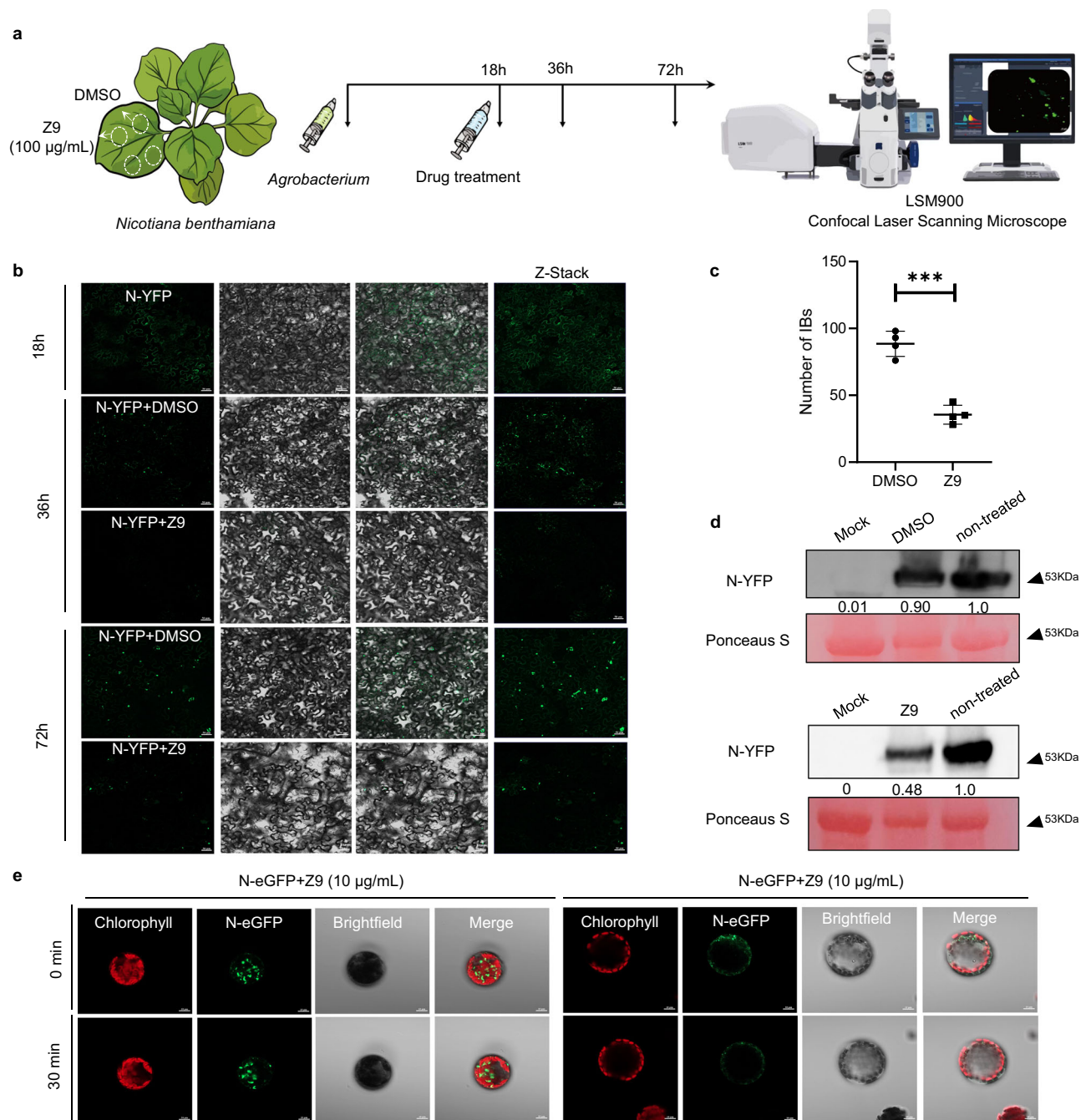


**Fig. 3 | Compound Z9 significantly disrupt the formation of IBs. a** Schematic method of exploring the effect of compound **Z9** on the formation of IBs in vivo. **b** Representative fluorescence images showing compound **Z9** could significantly reduce the formation of IBs in *N. benthamiana* leaves. DMSO was used as a control. The experiments were repeated at least three times with similar results. Bars, 50 µm. **c** The total number of IBs in confocal images at 72 h. Data are shown as individual data points and mean  $\pm$  SD ( $n = 4$ ). Statistical  $P$ -values were calculated using the two-tailed independent samples  $t$  test ( $P = 0.0001$ ),  $***, P < 0.001$ .

**d** Western blot was used to detect the accumulation level of protein N-YFP in the infiltrated leaves. Staining of RuBisCO with Ponceau S was used as a sample loading control. *N. benthamiana* plants were infiltrated with *Agrobacterium* containing empty vector (EV) as the mock control. The experiment was repeated three times with similar results. **e** Representative fluorescence images showing compound **Z9** could significantly degrade small IBs in *N. benthamiana* protoplasts. Bars, 10 µm. The experiment was repeated three times with similar results. Source data are provided as a Source Data file.

Encouraged by these bioinformatic insights, we pursued experimental verification to discern whether N protein condensates could indeed engage in phase separation activities. To this end, a construct encoding N-YFP was transiently expressed in *N. benthamiana* leaves. We observed that after 36 h, the N protein formed a relatively large number of small particles within the leaves, and by 72 h, the particles had significantly increased in size, but their number had significantly decreased (Fig. 4a). Time-lapse confocal imaging revealed these large

inclusions at 36 h occasionally divided slowly, spawning smaller ones that dispersed (Fig. 4b and Supplementary Movie 2). Indeed, the behavior of small, dynamic inclusions that frequently merged and coalesced into larger formations (Fig. 4c and Supplementary Movie 3). The characteristics of these inclusions, such as their sphericity, motility, and fusion/fission, as observed in N-YFP-infected cells, reveal that the IBs may exhibit properties akin to those of liquid droplets. At 36 h, the small IBs exhibited high-speed mobility within the cells, making it

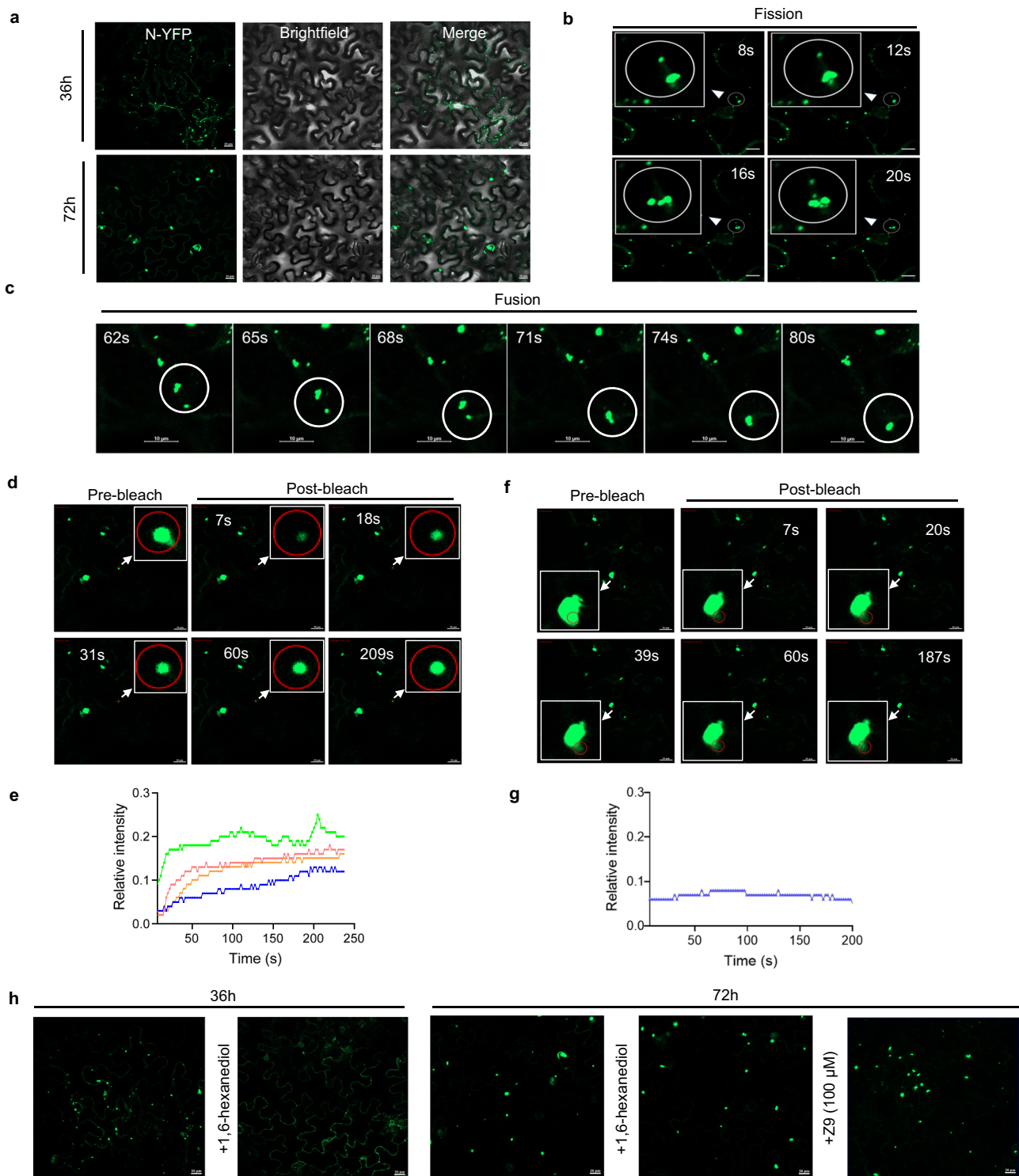


**Fig. 4 | N protein condensates possess gel-like phase separation properties.**

**a** The granule size of N-YFP formed in the *N. benthamiana* leaf cells at 36 hpi and 72 hpi. **b** Fluorescence time-lapse confocal images showing the fission of IBs. The white circles indicated the IBs undergoing fission at 36 hpi. Bars, 10  $\mu$ m. **c** Fluorescence time-lapse confocal images showing the fusion of IBs. The white circles indicated the IBs undergoing fusion at 36 hpi. Bars, 10  $\mu$ m. **d** Fluorescence recovery after photobleaching (FRAP) of small IBs formed in *N. benthamiana* cells. The images were taken every 2.5 s for 240 s to document fluorescence recovery, each time point was normalized to before photobleaching. Bars, 20  $\mu$ m. **e** Quantification of

the small N-YFP condensates in FRAP assays. ( $n = 4$  puncta). **f** Fluorescence recovery after photobleaching (FRAP) of large IBs formed in *N. benthamiana* cells. The images were taken every 2.5 s for 220 s to document fluorescence recovery, each time point was normalized to before photobleaching. Bars, 20  $\mu$ m. **g** Quantification of the large N-YFP condensates in FRAP assays. ( $n = 1$  puncta). **h** The effect of 1,6-hexanediol on N-YFP granules at 36 hpi and 72 hpi, and the effect of compound **Z9** on N-YFP granules at 72 hpi. The experiments were repeated at least three times with similar results. Bars, 20  $\mu$ m. Source data are provided as a Source Data file.



difficult to perform fluorescence recovery after photobleaching (FRAP) experiments. However, at 72 h, the particle mobility was significantly reduced. The results of the FRAP assay indicated that, after 72 h, the fluorescence intensity of small individual puncta was recovered, whereas the intensity of large individual puncta was difficult to recover (Fig. 4d–g).

Typically, phase-separated proteins achieve a photobleaching recovery rate of over 80%, but we observed consistently low levels of recovery (~10% to ~30%), which seems to indicate that the N protein condensates tend towards gel-like properties. To further confirm this, we conducted FRAP experiments with N-eGFP puncta from protoplasts, and the results revealed that complete bleaching of small individual puncta occurred at similarly low levels (~10% to ~30%), and large puncta were difficult to recover (Supplementary Fig. 5b–e). This phenomenon is consistent with linker histone H1 in the chromatin or Early Heading Date 6 (EHD6), which can bind to nucleic acids to form RNP<sup>58,59</sup>. To further explore whether these granules possess phase-separated properties, we treated the samples with 1,6-hexanediol, and the results revealed that treating the leaves at 36 h led to a significant reduction in particle number, whereas treating the leaves at 72 h made it difficult to observe a significant decrease in the number of large particles. Concurrently, we also treated the leaves with compound **Z9** and found that large particles were hard to eliminate (Fig. 4h). The phenomenon is consistent with the treatment of large N-eGFP particles in protoplasts (Fig. 3e). Together, these data demonstrate that the N protein undergoes phase separation from the surrounding cytoplasm, forming small phase-separated condensates with gel-like properties or transitions into larger solid-like granules, whereas compound **Z9** is more effective in the early stages and has difficulty disrupting the formation of large granules.

### The absence of potential binding sites reduces the proliferation of viruses in vivo

To explore how compound **Z9** affects the reduction of N protein condensates, we investigated the key binding sites of compound **Z9** on the N protein. We used different molecular docking software to predict the binding sites of compound **Z9** with the N protein and found that compound **Z9** could potentially interact with amino acids Arg94 (R<sup>94</sup>) and Tyr184 (Y<sup>184</sup>) (Fig. 5a and Supplementary Fig. 6a, b). TSWV N protein possesses a compact central domain, flanked by extended N- and C-terminal lobes on either side, forming a positively charged groove that is essential for RNA binding<sup>28,60</sup>. In the crystal structure of the N protein trimer complexed with nucleic acid (PDB ID: 5IP3), amino acids R<sup>94</sup> and Y<sup>184</sup> of each chain interact with the nucleic acid<sup>61</sup>. Further analysis revealed that the position at which **Z9** interacts with RNA in the N protein has a high degree of overlap (Supplementary Fig. 6c). To validate the effects of the potential binding sites of compound **Z9** on RNP proliferation, reverse PCR amplification and recombination were employed to construct the SR<sup>(+)</sup>eGFP<sup>R94A</sup>, SR<sup>(+)</sup>eGFP<sup>G147A</sup>, SR<sup>(+)</sup>eGFP<sup>Y184A</sup>, and SR<sup>(+)</sup>eGFP<sup>R94A&Y184A</sup> mini-replicons (Fig. 5b and Supplementary Fig. 7a–c). *N. benthamiana* plants were then infected using a competent minigenome replication system (RNP<sub>eGFP</sub>), and fluorescence was observed on the 5<sup>th</sup> day. The results showed that the absence of the amino acid R<sup>94</sup> marginally reduced the fluorescence level. Conversely, the absence of G<sup>147</sup> did not alter the intensity of fluorescence in leaf cells, whereas the absence of Y<sup>184</sup> or R<sup>94</sup>&Y<sup>184</sup> diminished fluorescence levels (Fig. 5c). The average fluorescence intensity was analyzed according to three independent biological replicates. The results revealed that RNP<sub>eGFP</sub><sup>WT</sup> and RNP<sub>eGFP</sub><sup>G147A</sup> had the strongest average fluorescence intensity in leaf cells (*t* test, *P* = 0.3054), RNP<sub>eGFP</sub><sup>R94A</sup> slightly decreased (*t*-test, *P* = 0.0064), and RNP<sub>eGFP</sub><sup>Y184A</sup> was the weakest among all single-point mutations (*t* test, *P* = 0.0001). Compared with the control, RNP<sub>eGFP</sub><sup>R94A&Y184A</sup> weakened more significantly (*t* test, *P* < 0.0001) (Fig. 5d). Additionally, the accumulation levels of N protein were further detected. Compared with RNP<sub>eGFP</sub><sup>WT</sup>, the lack of Y<sup>184</sup> or R<sup>94</sup>&Y<sup>184</sup>

significantly reduced the accumulation level of N protein, whereas the absence of R<sup>94</sup> slightly reduced the accumulation of N protein (Fig. 5e).

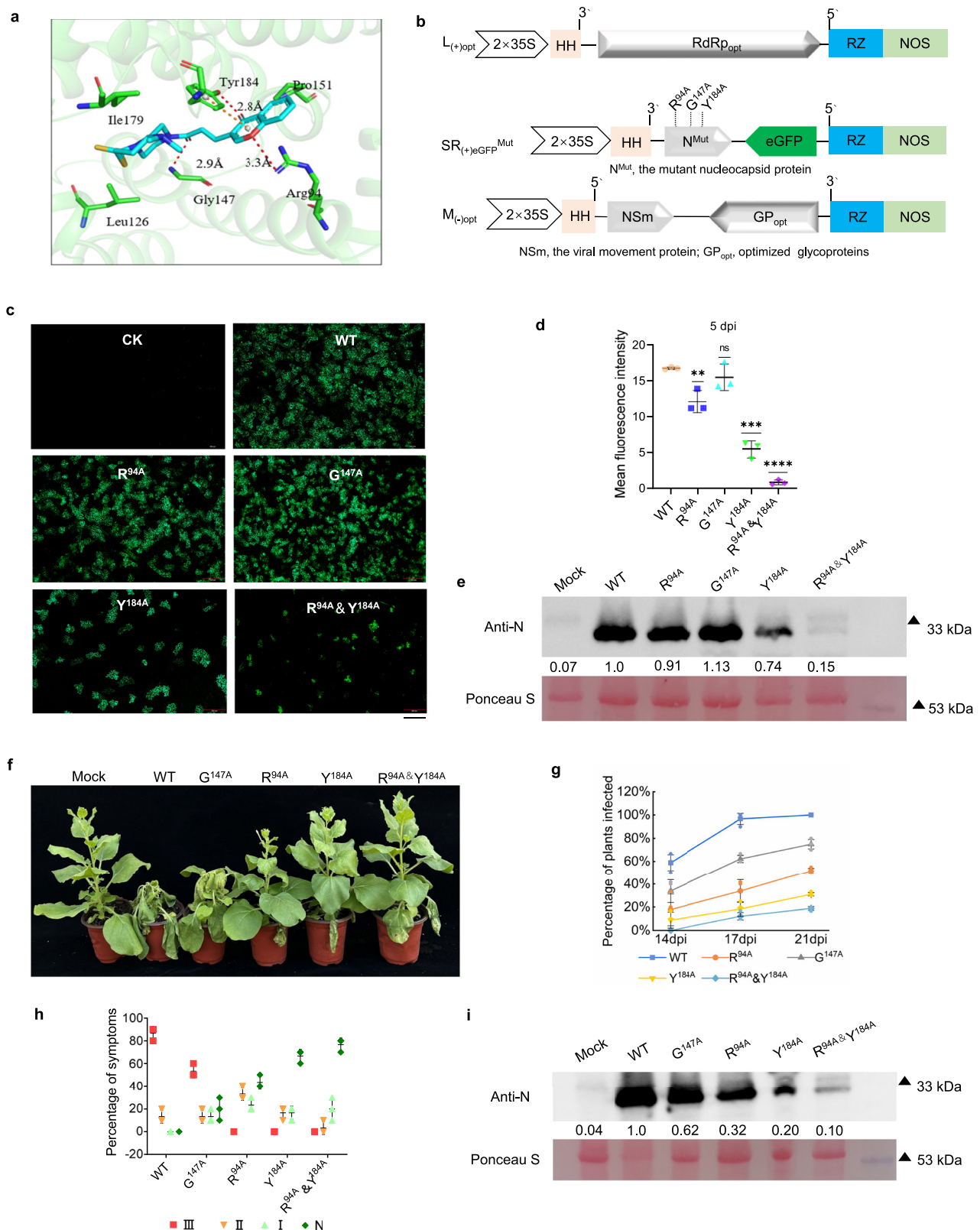
To verify the impact of missing binding sites on TSWV pathogenicity in plants, the movement-competent minigenome replication system (M<sub>(-)opt</sub>) was added to complement the cell-to-cell and systemic movements of reconstituted ribonucleoprotein complexes (RNPs). By the 14<sup>th</sup> day, noticeable pathogenic symptoms, such as leaf wrinkling and spotting, were evident in the systemic leaves of TSWV<sup>WT</sup>-infected plants. The severity of symptoms in TSWV-infected plants was divided into three grades (Supplementary Fig. 8a, b). By the 21<sup>st</sup> day, nearly all of the plants had significant wilting and mortality (grade III), with a disease susceptibility rate of 100%. In the case of TSWV<sup>G147A</sup>, more than 50% of the plants displayed severe disease symptoms (grade III) in systemic leaves, with an overall infection rate surpassing 70%. These findings suggest that the absence of G<sup>147</sup> somewhat delayed the systemic infection of plants by the virus. For TSWV<sup>R94A</sup> or TSWV<sup>Y184A</sup>, symptom onset in system leaves was slower and considerably milder than that of TSWV<sup>WT</sup>, with a susceptibility rate of approximately 50% (grade I and grade II). In contrast, plants infected with TSWV<sup>R94A&Y184A</sup> presented fewer spots on systematic leaves and a lower incidence rate of approximately 20% (grade I and grade II). Therefore, through a comprehensive comparative analysis of symptoms and infection rates, we found that the sole absence of R<sup>94</sup> or Y<sup>184</sup> effectively hindered the virus's systemic spread, and their combined absence drastically reduced it (Fig. 5f–h). The order of N protein accumulation level in the infected system leaves was TSWV<sup>WT</sup> > TSWV<sup>G147A</sup> > TSWV<sup>R94A</sup> > TSWV<sup>Y184A</sup> > TSWV<sup>R94A&Y184A</sup> (Fig. 5i). Further treatment of TSWV<sup>WT</sup> and TSWV<sup>R94A&Y184A</sup> with compound **Z9** revealed that the pathogenic symptoms of TSWV<sup>WT</sup> were significantly improved, whereas those of TSWV<sup>R94A&Y184A</sup> remained unchanged (Supplementary Fig. 8c). Together, these findings underscore that compound **Z9** may target nucleic acid binding sites and exert a crucial impact on viral proliferation in vivo by affecting RNP replication.

### Condensates are beneficial for the stability of the N protein

To further explore the interaction between compound **Z9** and the N protein, mutant proteins (N<sup>R94A</sup>, N<sup>Y184A</sup>, and N<sup>R94A&Y184A</sup>) were obtained via prokaryotic expression and purification (Supplementary Fig. 9a, b). BLI was employed to examine the binding dynamics between compound **Z9** and the N protein. Compared with that of N<sup>WT</sup> (7.6 μM), the affinity ability of compound **Z9** for the double mutant N<sup>R94A&Y184A</sup> was significantly diminished, with a *K*<sub>D</sub> value exceeding 400 μM (Fig. 6a). The microscale thermophoresis (MST) results indicated that the affinity constants of N<sup>R94A&Y184A</sup> with compound **Z9** decreased 180-fold (Fig. 6b). Similarly, the affinity constants for the single mutant proteins N<sup>R94A</sup> and N<sup>Y184A</sup> with compound **Z9** were reduced by approximately 103 and 135 times, respectively (Supplementary Fig. 9c, 9d). To further verify that the absence of the binding sites affects the interaction between the N protein and **Z9**, a labeling experiment was performed by incubating equal amounts of the probe with equimolar concentrations of N<sup>WT</sup> and N<sup>R94A&Y184A</sup>. We found the probe that N<sup>WT</sup> captured significantly more than that of N<sup>R94A&Y184A</sup> (Fig. 6c). These results indicate that mutations at residues (R<sup>94</sup> and Y<sup>184</sup>) within the nucleic acid binding region of the N protein significantly reduced the binding affinity of the compound **Z9**, suggesting that **Z9** targets the nucleic acid binding region of the N protein.

To investigate the influence of potential binding sites on the formation of IBs, we engineered a construct in which the N<sup>R94A&Y184A</sup> protein was transformed into a yellow fluorescent protein (N<sup>R94A&Y184A</sup>-YFP) (Supplementary Fig. 10a–c). When transiently expressed in *N. benthamiana* leaves, N<sup>WT</sup>-YFP formed numerous discrete cytoplasmic inclusions; in stark contrast, N<sup>R94A&Y184A</sup>-YFP was predominantly dispersed throughout the cytoplasm at 36 h, indicating a diffuse distribution pattern. At 72 h post-treatment, we observed that N<sup>WT</sup>-YFP





condensed into larger particles, whereas the distribution of  $N^{R94A \& Y184A}$ -YFP was significantly diminished (Fig. 6d). Western blot analysis revealed that the accumulation level of  $N^{R94A \& Y184A}$ -YFP markedly decreased after 72 h, suggesting that  $N^{R94A \& Y184A}$ -YFP might be degraded within the plant (Fig. 6e). These observations suggest that mutations at binding sites markedly decrease IB formation and are essentially consistent with the phenomenon of adding compound **Z9**.

To verify whether the stability of the N protein was reduced after the  $R^{94}$  and  $Y^{184}$  mutations, we conducted a protein stability assay. The results indicated that  $N^{WT}$ ,  $N^{R94A}$ , and  $N^{Y184A}$  maintained relatively good stability over different time periods, whereas  $N^{R94A \& Y184A}$  tended to degrade (Fig. 6f), implying that  $N^{R94A \& Y184A}$  is more susceptible to degradation in the body. During this process,  $N^{R94A \& Y184A}$ -YFP never formed many particles within the cells. Considering that  $N^{R94A \& Y184A}$ -YFP

**Fig. 5 | The potential binding sites of compound **Z9** and N protein significantly affect the replication of RNP and the proliferation of TSWV.** **a** Analysis of binding sites of compound **Z9** and N protein by molecular docking. **b** Schematic representation of constructs expressing TSWV full-length antigenomic  $L_{(-)opt}$  with optimized RdRp, full-length genomic  $M_{(-)opt}$  with optimized glycoproteins (GP) and the viral movement protein (NSm), full-length antigenomic  $SR_{(+eGFP}^{Mut}$ , and the sequence encoding amino acids ( $R^{94A}$ ,  $G^{147A}$ ,  $Y^{184A}$ , or  $R^{94A}\&Y^{184A}$ ) on the N protein gene were mutated to that of alanine. Minus sign (–) and 5' to 3' designation indicate the genomic RNA of TSWV. **c** Constructs ( $L_{(+)}opt + SR_{(+eGFP}^{WT}$ ) or its mutant ( $L_{(+)}opt + SR_{(+eGFP}^{Mut}$ ) with three RNA silencing virus inhibitors VSRs (P19, Hc-Pro, and Yb) co-expression in plants together with at least three plants in each experiment, the expression of eGFP protein in leaves was observed by fluorescence microscope on the 5<sup>th</sup> day. Bars, 500  $\mu$ m. **d** The average fluorescence intensities in infiltrated leaves on the 5<sup>th</sup> day) was measured by ImageJ. Error bars indicate  $\pm$  SD of the mean three independent experiments ( $n = 3$ ). Statistical  $P$ -values were calculated using the two-tailed independent samples  $t$ -tests (\*\*,  $P < 0.01$ ; \*\*\*,  $P < 0.001$ ; \*\*\*\*,  $P < 0.0001$ ; ns,  $P > 0.05$  not significant).  $R^{94A}$  ( $P = 0.0064$ ),  $G^{147A}$  ( $P = 0.3054$ ),

$Y^{184A}$  ( $P = 0.0001$ ),  $R^{94A}\&Y^{184A}$  ( $P < 0.0001$ ). **e** The accumulation level of N protein in the infiltrated leaves was detected by western blot. Staining of RuBisCO with Ponceau S was used as a sample loading control. The experiment was repeated three times with similar results. **f** Phenotypes of TSWV<sup>WT</sup> and TSWV<sup>Mut</sup> (TSWV<sup>R94A</sup>, TSWV<sup>G147A</sup>, TSWV<sup>Y184A</sup>, or TSWV<sup>R94A\&Y184A</sup>) -infected plants on the 21<sup>st</sup> day. Constructs ( $L_{(-)opt} + SR_{(+eGFP}^{WT} + M_{(-)opt}$ ) or its mutant ( $L_{(-)opt} + SR_{(+eGFP}^{Mut} + M_{(-)opt}$ ) with three RNA silencing virus inhibitors VSRs (P19, Hc-Pro, and Yb) co-expression in plants together with at least ten plants in each experiment. **g** The infection rates of TSWV<sup>WT</sup> and TSWV<sup>Mut</sup> -infected plants on days 14, 17, and 21. Error bars indicate  $\pm$  SD of the mean three independent experiments ( $n = 3$ ). **h** The percentages of TSWV<sup>WT</sup> and TSWV<sup>Mut</sup> -infected plants with different disease symptom grades. Error bars indicate  $\pm$  SD of the mean three independent experiments ( $n = 3$ ). **i** The accumulation level of N protein in the systemic leaves was detected by western blot. Staining of RuBisCO with Ponceau S was used as a sample loading control. The experiment was repeated three times with similar results. Source data are provided as a Source Data file.

is subject to degradation in plants, we purified recombinant His-sfGFP-N<sup>WT</sup> from *Escherichia coli* and examined its aggregation under conditions of relatively high concentration and low salinity (Fig. 6g). Confocal microscopy analysis revealed no significant aggregation of the His-sfGFP-N<sup>WT</sup> protein. RNP granules assemble through phase separation of their molecular components, and RNA is thought to be a critical element for the sizing and composition of the condensates<sup>62–66</sup>. N protein is a nucleic acid-binding protein, and the condensates it forms are similar to some RNPs, possessing gel-like properties<sup>58,59</sup>. Considering these preliminary studies, our focus shifted to investigating whether nucleic acids could mediate the formation of condensates. To explore this possibility, total RNA was extracted from TSWV-infected *N. benthamiana* leaves. His-sfGFP-N<sup>WT</sup> displayed a phase transition in the presence of RNA, rapidly forming larger, aggregate-like structures at high concentrations of RNA. RNA extracted from healthy *N. benthamiana* could also induce the aggregation of N protein, indicating that the binding of N protein to RNA is not specific (Supplementary Fig. 11a), which is consistent with previous conclusion<sup>67</sup>. However, these condensates exhibited a solid-like physical state rather than a fluidic state (Supplementary Fig. 11b). This rapid solidification parallels phenomena observed in liquid-to-solid phase separation-induced *oskar* ribonucleoprotein granules or N-terminal Toll/interleukin-1 receptor (TIR) domain proteins<sup>68,69</sup>. Their formation depends not only on the aggregating protein but also on environmental factors, such as pH, salt concentration, crowding, and the presence of membranes and condensates<sup>70</sup>. To verify whether mutations at the binding sites  $R^{94}$  and  $Y^{184}$  in the N protein significantly affect RNA-induced N protein condensation, we generated His-sfGFP-N mutants by substituting the residues with alanine residues  $R^{94A}/Y^{184A}$  (His-sfGFP-N<sup>R94A\&Y184A</sup>). Confocal microscopy data revealed that both the number and size of N protein condensates were greatly reduced by binding site mutation (Fig. 6h). These results suggest that the stability of the N protein in plants is related to RNA-mediated N protein condensation.

### Compound **Z9** inhibits nucleic acid-mediated N protein condensation

To further investigate the impact of these specific amino acids on the ability of the N protein to bind RNA, a digoxigenin-labeled RNA probe was prepared, and an electrophoretic mobility shift assay (EMSA) was conducted. We found that in the presence of N<sup>WT</sup>, the rate of RNA migration began to change slightly at a protein dosage of 0.1  $\mu$ g, with a significant decrease observed at dosages exceeding 0.1875  $\mu$ g. Conversely, for the N<sup>R94A\&Y184A</sup> mutant, a slight slowing in RNA migration was noted at a protein dosage of 1.5  $\mu$ g, with a substantial decrease only evident at dosages greater than 3.0  $\mu$ g (Supplementary Fig. 11c). These results indicate that the absence of these binding sites significantly

compromises the RNA binding capability of the N protein. We next immobilized biotin-labeled RNA (100 nM) onto streptavidin (SA) biosensors, and the binding affinities of N<sup>WT</sup> and N<sup>R94A\&Y184A</sup> with RNA were measured via BLI assay. The results suggested that the affinity constants (KDs) for N<sup>WT</sup> and N<sup>R94A\&Y184A</sup> binding to RNA were 7.3 nM and 36 nM, respectively (Fig. 7a, b), indicating that the mutation reduced the RNA-binding affinity of the N protein by approximately 5-fold. We observed that N<sup>WT</sup> exhibited faster association kinetics and slower dissociation kinetics compared to N<sup>R94A\&Y184A</sup> at low concentrations. Furthermore, when the biosensor was continuously loaded with N<sup>R94A\&Y184A</sup> and N<sup>WT</sup>, a significant increase in the binding curve was detected (Fig. 7c). Upon reversing the loading sequence, the binding curve decreased significantly (Supplementary Fig. 11d). These findings demonstrate that the absence of these binding sites significantly impairs the RNA-binding capacity of the N protein.

To evaluate the binding efficiency of compound **Z9** with the N-RNA complex, we first determined the affinity constant ( $KD = 150 \mu$ M) between compound **Z9** and RNA (Supplementary Fig. 11e). The interaction between compound **Z9** and the N protein ( $KD = 7.6 \mu$ M) was significantly stronger than that of **Z9**-RNA, indicating a preference of compound **Z9** for binding to the N protein. In the competitive binding assay, we discovered that the binding signal value of the N protein and RNA (0.26 nm) was markedly greater than that of the mixture of compound **Z9** and N protein (0.17 nm) (Fig. 7d). The constants of the binding rate and dissociation rate revealed that prebinding of compound **Z9** to the N protein significantly blocked RNA binding. To further explore whether compound **Z9** could destabilize the N protein-RNA complex, a mixture of N<sup>WT</sup> and RNA or a mixture of N<sup>WT</sup>, RNA, and **Z9** was added to total protein extracts, with or without UltraNuclease, and incubated for different periods of time. The stability of the N protein was subsequently assessed by western blotting (Fig. 7e). We found that the addition of compound **Z9** indeed caused degradation of the N protein (N<sup>WT</sup> + **Z9** + RNA, one-tailed paired  $t$ -test, 30 min,  $P = 0.2867$ ; 100 min,  $P = 0.0199$ ; 160 min,  $P = 0.0039$ ), and the stability of the N protein significantly decreased after the removal of nucleic acids (N<sup>WT</sup> + RNA + UltraNuclease, one-tailed paired  $t$  test, 30 min,  $P = 0.0449$ ; 100 min,  $P = 0.0214$ ; 160 min,  $P = 0.0004$ ) (Fig. 7f, g). These results suggest that **Z9** can block the binding of the N protein to RNA, leading to the degradation of the N protein. Overall, it was confirmed that condensates are caused by the interaction between the N protein and RNA, and these condensates can protect the protein from being extensively degraded within the cell. Compound **Z9** is an inhibitor targeting N, which can act on the dilute phase of the N protein or non-solidified condensates, disrupting the formation of these condensates by interfering with the normal protein-nucleic acid interactions, thereby further accelerating the degradation of the N protein (Fig. 7h).

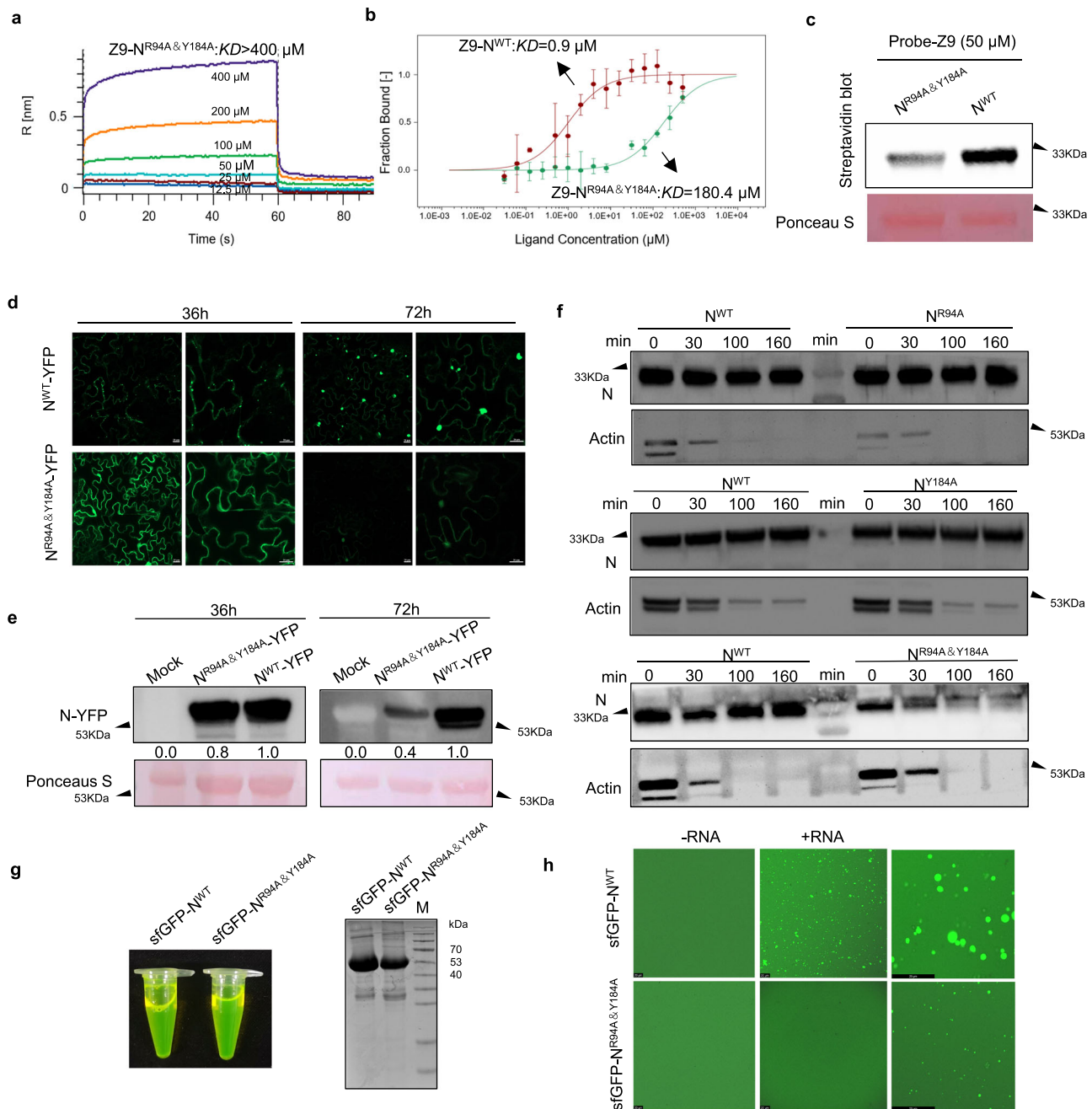


**Fig. 6 | The key binding sites significantly reduce the aggregation of N protein in vivo.** **a** The binding ability of compound **Z9** with N<sup>R94A&Y184A</sup> was measured by BLI. **b** The binding ability of compound **Z9** with N<sup>R94A&Y184A</sup> was measured by MST. The fitted curves and KD values calculated by Mo. Affinity Analysis (v.2.2.4). Each binding assay was repeated three times independently ( $n = 3$ ), and the bars represent SD. **c** Labeling experiment indicated that the probe bound by N<sup>WT</sup> significantly more than that of N<sup>R94A&Y184A</sup>. **d** Confocal micrographs showing the localization patterns of green fluorescence derived from N<sup>WT</sup>-YFP and N<sup>R94A&Y184A</sup>-YFP. Bars, 20  $\mu$ m. The experiments were repeated at least three times with similar results. **e** The accumulation level of N-YFP protein in the infiltrated leaves was detected by western blot. Staining of RuBisCO with Ponceau S was used as a sample loading control.

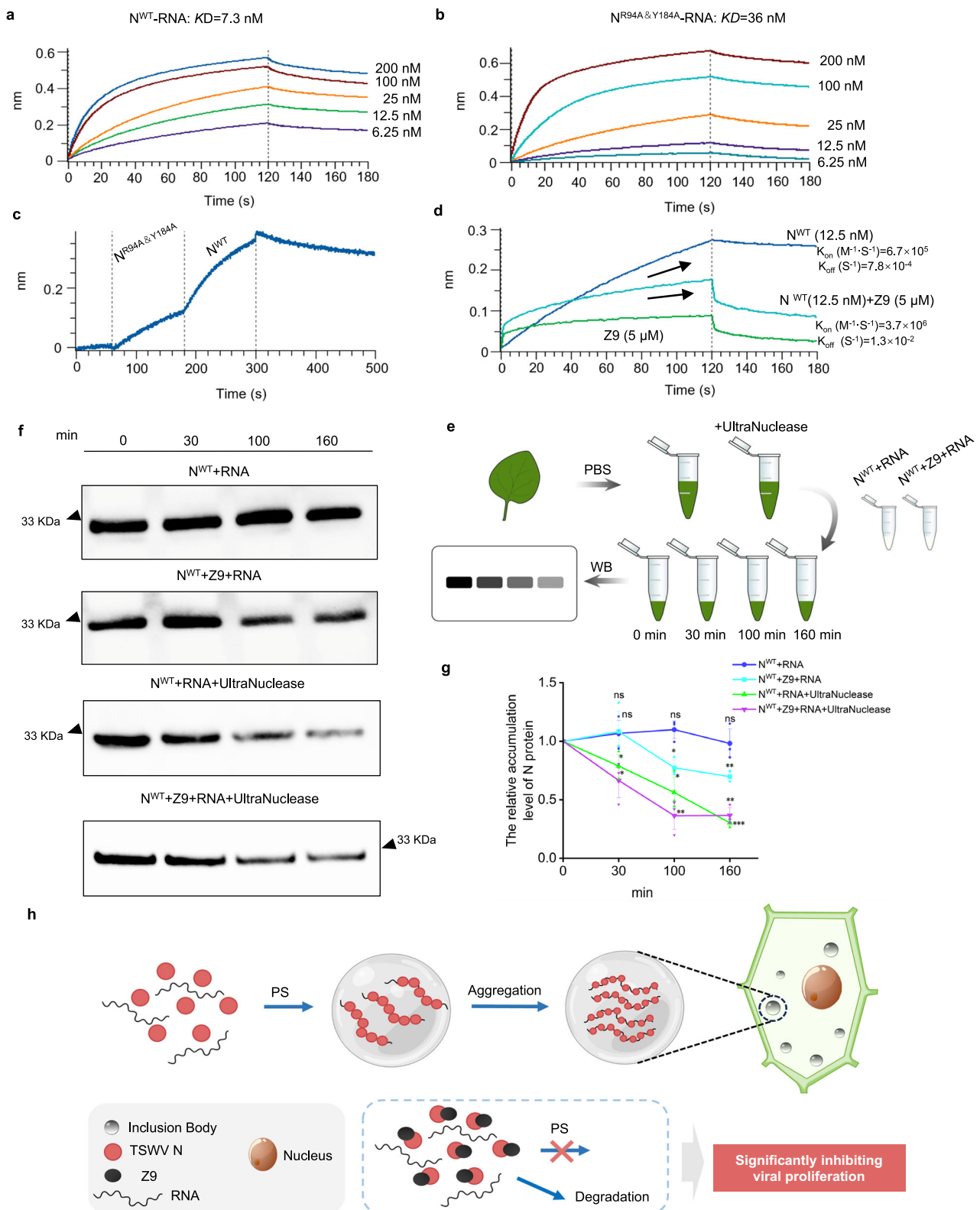
**f** Protein stability assay. Total protein was crudely extracted using PBS, allowed to stand at 0, 30, 100, and 160 min, and then the accumulation level of N protein was detected by western blot. Actin antibody was used as the internal control. **g** The purified protein (sfGFP-N<sup>WT</sup> or sfGFP-N<sup>R94A&Y184A</sup>) was identified by SDS-PAGE and showed green fluorescence. **h** R<sup>94</sup> and Y<sup>184</sup> mutations disrupt RNA mediated N condensate. The condensates of sfGFP-N<sup>WT</sup> and RNA were larger than that of sfGFP-N<sup>R94A&Y184A</sup> and RNA under the enlarged field of view. 50 ng/ $\mu$ L extracted RNA was incubated with 10  $\mu$ M sfGFP-N<sup>WT</sup> or sfGFP-N<sup>R94A&Y184A</sup> protein at 25 °C for 10 min. Bars, 20  $\mu$ m. The experiments were repeated three times with similar results. Source data are provided as a Source Data file.

## Discussion

Biomolecular condensate modulators have received much attention in the pharmaceutical field<sup>17–23</sup>; however, their application in agriculture remains highly limited. Consequently, based on the advantages of the privileged scaffold (benzopyrone and dithiocarbamate) in drug discovery<sup>36–43</sup>, a series of benzopyrone compounds were rationally

designed and synthesized by analyzing the structures of biomolecular condensate modulators in the pharmaceutical field (Fig. 1). We discovered that the introduction of amine groups into the side chain significantly improved the inhibitory activity of the compounds against TSWV (Table 1). Further investigations into the mechanism of action revealed that the highly active compound **Z9** could inhibit the





replication of viral RNPs (a complex of N protein, RNA, and RdRp) in vivo. Subsequent BLI screening indicated that the introduction of an amine group significantly improved the binding of the N protein to the compounds. The binding signal values were positively correlated with their activity to some extent, with compound **Z9** displaying the highest signal value (Fig. 2f). This suggests that the N protein is a potential target protein for **Z9**. The N protein is a direct target of **Z9** was further confirmed by pull-down of the probe (Supplementary Fig. 2). Currently, in

the drug discovery for treating plant viral diseases, the concentrations used in in vivo activity tests are relatively high, which may be related to the difficulty in control<sup>71</sup>. **Z9** shows better activity compared to other types of compounds against TSWV<sup>29,56,72,73</sup>. We found that **Z9** exhibits a certain degree of broad-spectrum antiviral activity against plant viruses due to the diverse biological activities of the privileged scaffolds, which indicates that **Z9** is a valuable lead compound. Through continuous optimization, it can provide an important research foundation for the



**Fig. 7 | Compound Z9 inhibits nucleic acid mediated N protein condensation.**

**a** The binding ability of RNA with N<sup>WT</sup> was measured by BLI. **b** The binding ability of RNA with N<sup>R94A&Y184A</sup> was measured by BLI. **c** Binding curve of continuous injection of N<sup>R94A&Y184A</sup> and N<sup>WT</sup> protein. **d** Competitive binding experiment confirmed that Z9 blocking the binding of RNA and N protein. The experiments were repeated three times with similar results. 5  $\mu$ M Z9 was first incubated with 12.5 nM N<sup>WT</sup> protein at 25 °C for 30 min, and then detected using SA sensors with fixed RNA. **e** The experiment where compound Z9 blocked the binding of protein N to RNA, leading to the degradation of protein N by proteases. In this experiment, protein N, RNA, and Z9 were incubated together at 25 °C for 30 min, then added to the total protein extracted from healthy leaf tissue in PBS buffer, and further incubated at 25 °C for 0, 30, 100, and 160 min respectively. Detection was carried out by immunoblotting. The use of an ultraNuclease to remove nucleic acids serves as a control. **f** The

accumulation level of N protein was detected by western blot. **g** Quantitative analysis of the accumulation levels of N protein in each treatment group using ImageJ. Each treatment was independently repeated in triplicate experiments. Error bars indicate  $\pm$  SD of the mean three independent experiments ( $n = 3$ ). Statistical  $P$ -values were calculated using the one-tailed paired samples  $t$ -tests (\*,  $P < 0.05$ ; \*\*,  $P < 0.01$ ; \*\*\*,  $P < 0.001$ ; ns,  $P > 0.05$  not significant). The same group of samples was compared for differences at three time points (30, 100, and 160 min) relative to 0 min. N<sup>WT</sup> + RNA (30 min,  $P = 0.2445$ ; 100 min,  $P = 0.0997$ ; 160 min,  $P = 0.4256$ ), N<sup>WT</sup> + Z9 + RNA (30 min,  $P = 0.2867$ ; 100 min,  $P = 0.0199$ ; 160 min,  $P = 0.0039$ ), N<sup>WT</sup> + RNA + UltraNuclease (30 min,  $P = 0.0449$ ; 100 min,  $P = 0.0214$ ; 160 min,  $P = 0.0004$ ), N<sup>WT</sup> + Z9 + RNA + UltraNuclease (30 min,  $P = 0.0427$ ; 100 min,  $P = 0.0086$ ; 160 min,  $P = 0.0027$ ). **h** Proposed model for Z9 as phase-separated (PS) biomolecular condensate inhibitor. Source data are provided as a Source Data file.

subsequent development of candidate compounds that remain effective at low concentrations and are cost-effective.

N protein is capable of forming highly motile cytoplasmic IBs that traffic on actin filaments, and partially colocalize with processing bodies (PBs) and stress granules (SGs), which is important for the TSWV<sup>33–35</sup>. When the N-YFP protein was transiently expressed in plants and treated with compound Z9, a significant reduction in the number of N protein condensates was observed (Fig. 3a–d and Supplementary Fig. 3). Furthermore, N-eGFP was expressed in protoplasts, and changes in condensates in specific cells after treatment with compound Z9 over time were observed. Large granules were difficult to eliminate, while the number of small granules significantly decreased (Fig. 3e). Considering that Z9 possess good inhibitory activity against the other plant viruses, we further explore whether Z9 could eliminate the other viral proteins. The binding constant of Z9 with PMMoV CP was 18  $\mu$ M, indicating a good binding capability. However, we found that the CP in the dilute phase did not seem to show a significant decrease, while Z9 could significantly reduce the number of TSWV N protein condensates in cells (Supplementary Fig. 4). This suggests that Z9 has a unique mechanism of action against TSWV. Recent study indicated that drugs are more easily recruited to condensates with phase separation to enhance their efficacy, rather than dilute phases<sup>74</sup>. This may provide a reasonable explanation for Z9 could more effectively target N protein condensates. Phase separation is recognized as a fundamental principle driving the formation of condensates<sup>3–6</sup>. Based on these results, we explored the formation process of these condensates and found that at 36 h, the granules were numerous and small, and by 72 h, the granules were increasingly larger, with further observation revealing a process of fusion (Fig. 4a–c). FRAP experiments revealed that the small granules mostly possessed gel-like phase separation properties, whereas larger granules are mostly in the solid state. Treatment with 1,6-hexanediol also affected the small granules, whereas the large granules seemed unaffected. Moreover, treatment with compound Z9 had little effect on large particles (Fig. 4h). These results elucidate the role of compound Z9 designed with CADs in the early stages of condensate formation, which includes the dilution phase and the process of small granules fusing to form larger granules. Currently, in the existing research on phase separation modulators, the pathogenic condensates targeted possess liquid-like properties, and drugs mostly serve to harden them or blocking interactions between macromolecules<sup>18–21</sup>. Similar to the condensates formed by TSWV N in vivo, some condensates are found to develop characteristics of gel-like properties or undergo a phase transition to a solid state<sup>58,59,68,69</sup>, and there is a significant lack of drug discovery for similar pathogenic condensates. A recent study has indicated that gel-droplets have a higher affinity for drugs than liquid-droplets, facilitating drug distribution<sup>75</sup>; in fact, the physicochemical properties of drugs and condensates play a key role in the distribution of drugs to the condensates where their targets reside<sup>76</sup>. We discovered that the introduction of basic amine groups is critical, enabling their classification as pH-responsive drugs (CADs), which significantly alters the

physicochemical properties of Z9. Our observations show that most biomolecular condensate inhibitors identified through high-content screening methods in the medical field possess alkaline groups<sup>20,42–46</sup>. Research has increasingly emphasized that physiological pH plays a significant role in regulating the formation of certain biomolecular condensates<sup>51–54</sup>, and of course, such studies involve the physiological environment inside cells, which adds to the complexity. As the mechanisms of condensate formation are increasingly discovered<sup>77</sup>, how to consider the physiological pH of condensate formation during the rational design of drug structures is highly important for the further development of biomolecular condensate modulators.

To further elucidate the mechanism of action of compound Z9, we found that the amino acids targeted by compound Z9 likely tend to be in the regions associated with nucleic acid binding. Further experimental results indicated that the absence of these potential binding sites (R<sup>94</sup> and Y<sup>184</sup>) significantly inhibited the replication of RNP and alleviated the pathological symptoms of TSWV, which was consistent with the mode of action of Z9 (Fig. 5b–i). In vivo experiments demonstrated that at 36 h, the absence of R<sup>94</sup> and Y<sup>184</sup> led to a diffuse distribution of the N protein within the cell, significantly reducing the number of condensates. Interestingly, after 72 h, N<sup>R94A&Y184A</sup>-YFP seemed difficult to observe, and immunoblot experiments confirmed that the accumulation level of the mutated protein was significantly reduced (Fig. 6d–f). These findings suggest that N<sup>R94A&Y184A</sup>-YFP is more prominently degraded in plants. This degradation mechanism could be a way for plants to recognize and degrade pathogen effector proteins through their protein degradation mechanisms, preventing their function within plant cells<sup>78</sup>. Therefore, we speculate that the formed condensates favor the stability of the N protein. We further found that sfGFP-N<sup>WT</sup> alone does not spontaneously form condensates, but the addition of nucleic acids rapidly induces the aggregation of the N protein, and under the same conditions, the aggregation ability of sfGFP-N<sup>R94A&Y184A</sup> is significantly reduced (Fig. 6f). Thus, these condensates are not solely the N protein, but likely RNP particles formed after the N protein binds to nucleic acids. The addition of compound Z9 inhibited the binding of the N protein to RNA (Fig. 7d). We further designed experiments to verify that reducing nucleic acids or adding compound Z9 increased the susceptibility of the N protein to degradation (Fig. 7e–g). Thus, through comprehensive research, condensates were confirmed to form through the interaction of the N protein with RNA, and this condensate plays a protective role for the protein. Compound Z9, an inhibitor that targets condensates, disrupts the formation of these condensates by directly blocking protein–nucleic acid interactions, further leading to the degradation of the N protein. Under normal circumstances, more attention is paid to the protective role of RNPs on nucleic acids, as well as transcription and translation<sup>65,66</sup>. A recent study found that phase-separated condensates can reduce protein degradation by compartmentalizing components of the proteasome machinery<sup>79</sup>. Leveraging the cell's innate protein degradation systems to selectively degrade disease-associated pathogenic proteins represents an important strategy in

drug development<sup>80,81</sup>. The utilization of protein degradation systems to disrupt pathogenic condensates has begun to attract attention in the pharmaceutical field<sup>82–84</sup>.

Previous studies have shown that the N proteins of other viruses belong to the family *Tospoviridae* have an identical mechanism of RNA encapsidation with TSWV N, with R<sup>94</sup> being highly conserved in *Tospoviruses* and Y<sup>184</sup> present in groundnut yellow spot virus (GYSV) and tomato chlorotic spot virus (TCSV)<sup>60,61</sup>. This suggests that **Z9** may be effective in preventing and controlling viruses in the family *Tospoviridae*. Based on the effect of **Z9** in disrupting the normal binding of N-RNA, how to design more effective drugs will arouse our interest. Given the increasing evidence that many plant viruses and phytopathogenic bacteria rely on the condensation of replication proteins for proliferation<sup>24–27,85</sup>, the discovery of biomolecular condensate inhibitors could play a significant role in controlling plant diseases that were hard to manage.

## Methods

### Materials and virus sources

The seeds of *N. glutinosa* and *N. benthamiana* were preserved by our laboratory. All of the plants were cultured in an artificial climate chamber (25 °C during the day, 50% relative humidity/23 °C at night, 40% relative humidity). The full-length infectious clone vectors (L<sub>(+)opt</sub>, M<sub>(-)opt</sub>, and SR<sub>(+)eGFP</sub>), the expression vector of silencing suppressors (VSRs), and vector pCambia2300-N-YFP were provided by Professor Xiaorong Tao (Nanjing Agricultural University). The TSWV lettuce isolate was maintained in *N. benthamiana*, and the infected leaves were maintained at –80 °C.

### Plasmid construction

To generate the mutant plasmids SR<sub>(+)eGFP</sub><sup>Mut</sup> (SR<sub>(+)eGFP</sub><sup>R94A</sup>, SR<sub>(+)eGFP</sub><sup>Y184A</sup>, SR<sub>(+)eGFP</sub><sup>G147A</sup>, and SR<sub>(+)eGFP</sub><sup>R94A&Y184A</sup>), the insertion fragments and vectors were obtained with SR<sub>(+)eGFP</sub><sup>WT</sup> as a template via reverse polymerase chain reaction. For the p2300-N<sup>R94A&Y184A</sup>-YFP construct, the cDNA of the N<sup>R94A&Y184A</sup> gene was amplified from SR<sub>(+)eGFP</sub><sup>R94A&Y184A</sup> and then inserted into the binary vector pCambia2300-YFP. The plasmid pAN580-N-eGFP was constructed by Biorun Biosciences Co., Ltd. (Wuhan, China). All of the constructs were verified via DNA sequencing. The primers used are shown in Supplementary Table 2.

### Synthesis

All commercial reagents and solvents were used without further purification. Thin layer chromatography (TLC) was performed on pre-coated silica gel GF254 plates. Visualization of TLC was achieved using UV light (wavelength of 254 nm). Column chromatography was performed on silica gel (300–400 mesh) using the proper eluent. NMR data were recorded on a Bruker DPX 400 MHz (Bruker, Germany). Chemical shifts were reported in parts per million (ppm) referenced to the appropriate solvent peaks ( $\delta$  7.26 ppm for CDCl<sub>3</sub> in the proton spectra, 77.0 ppm for CDCl<sub>3</sub> in the fully decoupled <sup>13</sup>C spectra). The following abbreviations were used to describe the peak splitting patterns: *s* = singlet, *d* = doublet, *t* = triplet, and *m* = multiplet. The coupling constants *J* are reported in Hertz (Hz). High-resolution mass spectra were obtained with a Thermo Scientific Q Exactive instrument (Thermo Scientific, USA). The specific synthesis steps can be found in Supplementary Method 1 and Supplementary Figs. 12–14, and the structural identification of the compounds can be found in Supplementary Note 1 and Supplementary Figs. 15–92.

### Anti-TSWV assay

Healthy *N. glutinosa* was used as the model plant, and the inhibitory activities of the compounds against TSWV were tested via the half-leaf method. For curative activity, carborundum powder was pre-coated on the leaves of the plant, and the extracted viral mixture was inoculated onto the leaves via a soft brush. After 30 min, the leaves were rinsed

thoroughly with water, and the agent was evenly applied to the right side of each leaf. For protective activity, the prepared agent was first evenly applied to the right side of the leaves. After 12 h, the extracted viral mixture was inoculated onto the leaves. For inactivation activity, the prepared agent with an equal amount of extracted virus mixture was diluted on ice, and the mixture was inoculated onto the right leaves after 30 min. At that time, the extracted virus was diluted with the same amount of buffer solution and inoculated onto the left leaves. The plants were subsequently placed in an artificial climate chamber (25 °C during the day, 50% relative humidity/23 °C at night, 40% relative humidity) for cultivation. The number of lesions was counted after approximately 2 days. For the EC<sub>50</sub> test of inactivation activity, the concentrations of the compounds were set to 31.25, 62.5, 125, 250, and 500 µg/mL. The method is consistent with the description provided above. The extracted TSWV was inoculated on the lower leaves of the tomatoes. The plants were cultured in an artificial climate chamber (25 °C during the day, 50% relative humidity/23 °C at night, 40% relative humidity). After 24 h, 100 µg/mL agent (2.0 mg of compound **Z9**, 50 µL of DMSO, 20 mL of 2% (v/v) Tween 80 water) was sprayed onto the tomato leaves, with 20 mL of 3% Tween 80 water containing DMSO (50 µL) as a control. Pathogenic symptoms were observed after ~20 days.

**Agrobacterium infiltration.** *Agrobacterium tumefaciens* strain GV3101 was transfected with the recombinant plasmids, and the monoclonal clone was selected and cultured at 28 °C for approximately 24–36 h. *A. tumefaciens* cells were resuspended in agroinfiltration buffer (10 mM MES, pH = 5.6, 10 mM MgCl<sub>2</sub>, and 100 µM acetosyringone) and incubated for 2 to 3 h in the dark at room temperature after the optical density at 600 nm (OD<sub>600</sub>) was adjusted. The cells were used for agroinfiltration of *N. benthamiana* leaves. For the competent mini-genome replication system (L<sub>(+)opt</sub> + SR<sub>(+)eGFP</sub> + VSRs) or reconstituted infectious TSWV (L<sub>(+)opt</sub> + SR<sub>(+)eGFP</sub> + M<sub>(-)opt</sub> + VSRs), equal volumes of *Agrobacterium* cultures harboring the full-length infectious clone vector (final concentration OD<sub>600</sub> = 0.20) were mixed with the bacterial mixture (final concentration OD<sub>600</sub> = 0.05) containing the VSRs (P19-HcPro-yb)<sup>55</sup>. For the expression vector p2300-N-YFP, the cells were resuspended in an agroinfiltration buffer adjusted to an optical density (OD<sub>600</sub>) of 0.50. Leaves of *N. benthamiana* plants at the 5–6-leaf stage were infiltrated with *Agrobacterium* cultures using syringes. The infiltrated plants were grown in an artificial climate chamber. The operation of the mutants is consistent with the above description.

### Pull-down assay

TSWV-systemically infected leaves of *N. benthamiana* were collected, and extraction buffer (25 mM Tris-HCl, pH = 7.5, 150 mM NaCl, 1 mM EDTA, 2% w/v polyvinylpyrrolidone, 10 mM dithiothreitol, 0.5% v/v Triton X-100, 10% v/v glycerol, and 1 × protease inhibitor cocktail) was added to obtain the total crude protein extract. 10 µL of the probe solution (100 mM) was added into 1 mL of the total extracted protein solution and incubated in the dark for 2 h. Sequentially 25 µL of 10 mM N<sub>3</sub>-biotin, 10 µL of 100 mM BTAA, 10 µL of 100 mM CuSO<sub>4</sub>, and 5 µL of 500 mM vitamin C were added into the reaction system. After mixing, the system was reacted at 37 °C for 3 h. 0.5 mL of the treated magnetic beads were added into the mixture, and incubated for 12 h. After enrichment, the centrifuge tubes were placed on a magnetic stand, and the supernatant was used as the input group. The magnetic beads were washed with 0.5 mM PBS (containing 2 mM UA) and mass spectrometry water. Proteins bound to streptavidin beads were fractionated by SDS-PAGE and analyzed by immunoblotting using an N protein antibody. For the competitive binding experiment between compound **Z9** and the probe, 1.0 µL of 50 µM the probe and 20 µL of N protein (0.5 mg/mL) were incubated with different concentrations of compound **Z9** (50, 500, 1000, and 1500 µM) for 2 h. Sequentially 0.5 µL of 10 mM N<sub>3</sub>-biotin, 0.2 µL of 100 mM BTAA, 0.2 µL of 100 mM

CuSO<sub>4</sub>, and 0.1 μL of 500 mM vitamin C were added into the reaction system. After mixing, the system was reacted at 37 °C for 3 h. The mixture was fractionated by SDS-PAGE and analyzed by immunoblotting using HRP-Streptavidin (1:6000, Sangon Biotech, China, Cat. No. D11054).

### Isolation of protoplasts and transformation with N-eGFP

*N. benthamiana* protoplasts were prepared and transformed via the plant protoplast preparation and transformation kit (Real-Times, China). Briefly, 0.20 g of *N. benthamiana* leaves were cut into strips 0.5–1 mm in width, submerged in 10 mL of enzymatic hydrolysate [5 mL of solution I, 0.15 g of cellulose R-10, 0.04 g of pectinase R-10, 5 μL of β-mercaptoethanol, 0.2 mL of 50 mg/mL BSA] and treated at 20–25 °C for 3 h. The mixtures were then added to 10 mL of solution II and centrifuged at 100 × g at room temperature for 2 min, followed by resuspension in 1 mL of solution III. Five hundred microlitres of protoplast cells and 500 μL of transformation mixture were mixed and transfected with 75 μg of the pAN580-N-eGFP plasmid at room temperature for 15 min. After 16 h, the transformed protoplasts were resuspended in solution II and cultured in solution V at 25 °C for the expression of N-eGFP. The obtained protoplasts were detected via a confocal microscope with a ×63 oil immersion objective (Zeiss, Oberkochen, Germany).

### Drug treatments

When N-YFP was significantly expressed in the leaves of *N. benthamiana* after 18 h, the compound **Z9** (2.0 mg) was dissolved in 100 μL of DMSO, followed by the addition of 20 mL of ddH<sub>2</sub>O or 0.1% tween 80 aqueous solution to prepare a 100 μg/mL agent, which was rapidly injected into the infiltration area below the left side of the leaf. Concurrently, 0.5% DMSO (v/v) was injected into the infiltration area above the left side of the leaf. After 18 and 54 h, confocal microscopy with Z-Stack was used to capture micrographs of the left side drug-treated and right side of untreated areas within the same leaf. The drug treatment at 36 h is consistent with the description above. The treatment of PMMoV CP-YFP with the compound **Z9** was consistent with the above description. To determine the impact of drug treatment on N-eGFP in protoplasts, compound **Z9** was diluted to 200 μg/mL. Then, 10 μL of the drug mixture was quickly and evenly mixed with 200 μL of protoplasts, and a confocal microscope was immediately used to locate intact cells expressing N-eGFP. The effects of **Z9** on N-eGFP condensates were observed within 30 min.

### Fluorescence microscopy

Agro-infiltrated *N. benthamiana* leaves were examined for fluorescence expression via an OLYMPUS model BX53F fluorescence microscope (OLYMPUS, Tokyo, Japan) with a green barrier filter. The samples were fixed in water on a microslider under a coverslip to detect eGFP fluorescence. The fluorescence images were collected using CellSens Standard 1.18 (OLYMPUS, Tokyo, Japan).

### Confocal microscopy and fluorescence recovery after photobleaching

Confocal laser scanning micrographs of Agro-infiltrated leaves were captured with a Zeiss LSM900 confocal laser scanning microscope (Zeiss, Oberkochen, Germany). The fluorescent protein was excited at 488 nm, and time-lapse images were taken over a 1- or 2-min period. For fluorescence recovery after photobleaching (FRAP) experiments, IB droplets formed in infected leaf cells were bleached with a laser at 488 nm (50% or 100% intensity) under a confocal microscope with ×20 water immersion, and the field of view was magnified ×2.5. After bleaching, at least 40 frames of recovery images were collected in time-lapse mode. The images were collected and the fluorescence intensity of the bleaching region was measured via ZEN 3.1 (Zeiss, Oberkochen, Germany). The data were normalized, and recovery

curves were generated with GraphPad Prism 8 (GraphPad, San Diego, USA).

### Protein extracts and immunoblot assays

Healthy, Agro-infiltrated leaf patches or TSWV-systemically infected leaves of *N. benthamiana* were collected, and total protein was extracted in 1 mL of extraction buffer (25 mM Tris-HCl, pH = 7.5, 150 mM NaCl, 1 mM EDTA, 2% w/v polyvinylpyrrolidone, 10 mM dithiothreitol, 0.5% v/v Triton X-100, 10% v/v glycerol, and 1 × protease inhibitor cocktail)<sup>55</sup>. The samples were transferred to PVDF membranes after separation by SDS-PAGE. The membranes were blocked with 5% w/v skim milk solution and probed with a rabbit polyclonal anti-N antibody (1:5000, Donated by Professor Xiaorong Tao from Nanjing Agricultural University) or a rabbit polyclonal anti-PMMoV CP antibody (1:5000, Donated by Professor Fei Yan from Ningbo University). RuBisCO stained with Ponceau S was used as a sample loading control. Finally, the signal was visualized with a ChemiDoc MP Imaging System (Bio-Rad, Hercules, USA). Quantitative analysis was performed using ImageJ v1.52.

### Molecular docking

The binding sites of compound **Z9** with the protein in the TSWV N crystal structure (PDB: 5IPI) were predicted using Schrödinger maestro 13.5, LeDock, and AutoDock Vina 1.1.2 for the monomer. PyMOL was used as the plotting software.

### Protein purification and microscale thermophoresis (MST) assay

The prokaryotic expression vectors (pET-32a-N<sup>WT</sup>, pET-32a-N<sup>R94A</sup>, pET-32a-N<sup>Y184A</sup>, pET-32a-N<sup>R94A&Y184A</sup>, pET-21a-sfGFP-N<sup>WT</sup>, and pET-21a-sfGFP-N<sup>R94A&Y184A</sup>) were successfully introduced into *Escherichia coli* BL21 (DE3). The expression strains were induced by isopropyl-β-D-thiogalactopyranoside at 28 °C overnight, after which the precipitates were lysed (power 35%, 40 min, 4 s ultrasound, and 6 s interval) with buffer (0.869 g NaCl, 3.75 mL PBS, 36 μL mercaptoethanol, 5 mL glycerol, 41.25 mL H<sub>2</sub>O, pH = 7.4). The lysates were clarified by centrifugation at 16,000 × g for 30 min. The proteins were purified via affinity chromatography using a Trap high-performance column (GE Healthcare, USA). The binding affinities of compound **Z9** to the proteins were determined with a Monolith NT.115 instrument (NanoTemper, Munich, Germany). The Mo. Affinity Analysis 2.2.4 software (NanoTemper, Munich, Germany) was used to fit the MST curve and obtain the affinity constants (KD). The specific operation was performed according to the reported literature<sup>29</sup>.

### In vitro RNA-induced N protein aggregation

Total RNA from healthy or TSWV-infected *N. benthamiana* leaves was extracted with TRIzol and quantified at a concentration of 1000 ng/μL. The purified 6×His-tagged sfGFP-N<sup>WT</sup> or sfGFP-N<sup>R94A&Y184A</sup> was concentrated to 10 μM in desalting buffer (20 mM Tris-HCl, pH 7.5, and 150 mM NaCl). Twenty microlitres of protein and 2 μL or 1 μL of RNA were incubated for 10 min, and the mixture was observed with a confocal microscope.

### Electrophoretic mobility shift assay (EMSA)

The digoxigenin-labeled RNA probe was prepared following the previously described protocol<sup>31</sup>. Briefly, a DNA template with the T7 promoter sequence was generated via polymerase chain reaction and purified using a gel recovery kit. The RNA was then transcribed in vitro using T7 RNA polymerase (Promega, Madison, USA, Cat. No. P2075). One microlitre of RNA probe at a concentration of approximately 1200 ng/μL was placed in a PCR tube and diluted to 40 ng/μL with DEPC water. One microlitre of RNA probe (40 ng/μL) was added to the PCR tubes and mixed with 9 μL of different quantities of the purified N<sup>WT</sup> or N<sup>R94A&Y184A</sup> (0, 0.025, 0.05, 0.1, 0.1875, 0.375, 0.75, 1.5, or 3.0 μg). The mixtures were incubated in an ice water bath for 10 min. The samples



were transferred onto a nylon membrane. The membrane was exposed to UV light, probed with an anti-digoxin alkaline phosphatase antibody (1:5000, Roche, Basel, Switzerland, Cat. No. 11585614910) for 1–2 h, and then incubated with BCIP-NBT for staining at 37 °C. The signal was directly visualized and photographed.

### Biolayer interferometry (BLI) assays

The purified His-tagged N protein was loaded onto Ni-NTA biosensors, and the binding signal values of different compounds (50 µg/mL) were measured via a biolayer interferometry method with Octet RED 96 (ForteBio, San Francisco, USA). All of the compounds were diluted in PBST. The affinity constants (KD) between compound **Z9** and the recombinant wild-type and mutant proteins were measured using Octet BLI Discovery 12.2 (ForteBio, San Francisco, USA). The binding constants of compound **Z9** with proteins were determined via global fit analyses of experimental binding curves using the Octet Analysis Studio 12.2 (ForteBio, San Francisco, USA). To analyze the effects of binding sites on N-RNA interactions, 100 nM of biotinylated RNA (bio-GAGAGCAAUUGUGUCAGAA) was loaded onto streptavidin (SA) biosensors and balanced with PBS. The biosensors were then exposed to diluted recombinant N<sup>WT</sup> or N<sup>R94A&Y184A</sup>, followed by washing (dissociation) with PBS. The affinity constant (KD) values were calculated via Octet Red software. For the binding inhibition experiments, the affinity constant (KD) value of compound **Z9** with RNA was first measured via BLI, and compound **Z9** (5 µM) was then combined with the N protein (12.5 nM) and incubated for 30 min at room temperature. The biosensors were exposed to recombinant N protein (12.5 nM), incubated with a mixture of compound **Z9** and N protein, and then with compound **Z9** (5 µM), followed by washing (dissociation) with PBST. Association rate constants ( $K_{on}$ ) and dissociation rate constants ( $K_{off}$ ) were measured using Octet BLI Discovery 12.2 (ForteBio, San Francisco, USA).

### Protein stability

Systematically infected leaves (1.0 g) from plants infected with TSWV<sup>WT</sup>, TSWV<sup>R94A</sup>, TSWV<sup>Y184A</sup>, or TSWV<sup>R94A&Y184A</sup> were collected. A total of 1.0 mL of 5 mM PBS buffer (pH=8.0) was added, and the mixture was ground finely. Then, 100 µL of each mixture was added, and the mixture was distributed into 4 separate 1.5 mL centrifuge tubes. The samples were incubated at 25 °C for 0, 30, 100, or 160 min and then centrifuged at 13,198 × g for 10 min. Eighty microlitres of the supernatant from each sample was mixed with 20 µL of 5 × loading buffer and then denatured at 100 °C for 10 min. The accumulation level of N protein and actin (1:2000–5000, ABClonal, Wuhan, China, Cat. No. AC009) was detected via an immunoblotting assay. To test the ability of compound **Z9** to disrupt N-RNA binding and destabilize the N protein, 1.0 g of healthy leaf tissue was collected, and total protein was extracted with 1.0 mL of PBS. UltraNuclease (25 U/mL) was added to 0.5 mL of the extracted solution. Compound **Z9** (5 µM) was incubated with purified N<sup>WT</sup> (12.5 nM) and the above 100 nM biotin-labeled RNA at room temperature for 30 min and then added to 0.5 mL of the extracted mixture containing UltraNuclease. The same mixture (5 µM **Z9**, 12.5 nM N<sup>WT</sup>, and 100 nM RNA) was added to 0.5 mL of extracted solution without Omni-Nuclease as a control. After they were incubated at 25 °C for 0, 30, 100, and 160 min, they were denatured at 100 °C for 10 min. The accumulation level of N protein was detected by immunoblotting. The treatment without the addition of compound **Z9** followed the same procedure as described above.

### Data analysis

The data in the article was processed using Microsoft Office Excel 2019 or GraphPad Prism 8.0 software (GraphPad Software, San Diego, CA, USA). Statistically significant differences between groups were assessed using GraphPad Prism 8.0 software (GraphPad Software, San Diego, CA, USA). *P*-values were calculated using the two-tailed *t*-test or

one-tailed paired *t* test from triplicated independent experiments. Data are presented as mean ± standard deviation. Four levels of significance (\**p* < 0.05, \*\**p* < 0.01, \*\*\**p* < 0.001, \*\*\*\**p* < 0.0001) were used for all tests.

### Reporting summary

Further information on research design is available in the Nature Portfolio Reporting Summary linked to this article.

### Data availability

A reporting summary for this article is available as a Supplementary Information file. Data supporting the findings of this work are available within the paper and its Supplementary Information files. The crystal structure of the N protein used for molecular docking was downloaded from the Protein Data Bank with PDB code [5IP1](#). Source data are provided in this paper.

### References

- Banani, S. F., Lee, H. O., Hyman, A. A. & Rosen, M. K. Biomolecular condensates: organizers of cellular biochemistry. *Nat. Rev. Mol. Cell Biol.* **18**, 285–298 (2017).
- Mayr, C., Mittag, T., Tang, T.-Y. D., Wen, W., Zhang, H. & Zhang, H. Frontiers in biomolecular condensate research. *Nat. Cell Biol.* **25**, 512–514 (2023).
- Brangwynne, C. P. et al. Germline P granules are liquid droplets that localize by controlled dissolution/condensation. *Science* **324**, 1729–1732 (2009).
- Alberti, S. & Hyman, A. A. Biomolecular condensates at the nexus of cellular stress, protein aggregation disease and ageing. *Nat. Rev. Mol. Cell Biol.* **22**, 196–213 (2021).
- Sabari, B. R. et al. Coactivator condensation at super-enhancers links phase separation and gene control. *Science* **361**, eaar3958 (2018).
- Myong, S. & Shorter, J. Introduction: phase separation. *Chem. Rev.* **123**, 8943–8944 (2023).
- Li, P. et al. Phase transitions in the assembly of multivalent signalling proteins. *Nature* **483**, 336–340 (2012).
- Shin, Y. & Brangwynne, C. P. Liquid phase condensation in cell physiology and disease. *Science* **357**, eaaf4382 (2017).
- Alberti, S., Gladfelter, A. & Mittag, T. Considerations and challenges in studying liquid-liquid phase separation and biomolecular condensates. *Cell* **176**, 419–434 (2019).
- Gao, Y. et al. A brief guideline for studies of phase-separated biomolecular condensates. *Nat. Chem. Biol.* **18**, 1307–1318 (2022).
- Wu, C., Holehouse, A. S., Leung, D. W., Amarasinghe, G. K. & Dutch, R. E. Liquid phase partitioning in virus replication: observations and opportunities. *Annu. Rev. Virol.* **9**, 285–306 (2022).
- Li, H. et al. Phase separation in viral infections. *Trends Microbiol.* **30**, 1217–1231 (2022).
- Banerjee, I. et al. Influenza A virus uses the aggresome processing machinery for host cell entry. *Science* **346**, 473–477 (2014).
- Fang, J. et al. Spatial and functional arrangement of Ebola virus polymerase inside phase-separated viral factories. *Nat. Commun.* **14**, 4159 (2023).
- Charman, M. et al. A viral biomolecular condensate coordinates assembly of progeny particles. *Nature* **616**, 332–338 (2023).
- Cai, S. et al. Phase-separated nucleocapsid protein of SARS-CoV-2 suppresses cGAS-DNA recognition by disrupting cGAS-G3BP1 complex. *Sig Transduct. Target Ther.* **8**, 170 (2023).
- Mitrea, D. M. et al. Modulating biomolecular condensates: a novel approach to drug discovery. *Nat. Rev. Drug Discov.* **21**, 841–862 (2022).
- Ding, M., Xu, W., Pei, G. & Li, P. Long way up: rethink diseases in light of phase separation and phase transition. *Protein Cell* **15**, 475–492 (2023).



19. Conti, B. A. & Oppikofer, M. Biomolecular condensates: new opportunities for drug discovery and RNA therapeutics. *Trends Pharm. Sci.* **43**, 820–837 (2022).
20. Risso-Ballester, J. et al. A condensate-hardening drug blocks RSV replication in vivo. *Nature* **595**, 596–599 (2021).
21. Zhao, M. et al. GCG inhibits SARS-CoV-2 replication by disrupting the liquid phase condensation of its nucleocapsid protein. *Nat. Commun.* **12**, 2114 (2021).
22. Du, S., Hu, X., Liu, X. & Zhan, P. Revolutionizing viral disease treatment: Phase separation and lysosome/exosome targeting as new areas and new paradigms for antiviral drug research. *Drug Discov. Today* **29**, 103888 (2024).
23. Sake, S. M. et al. Drug repurposing screen identifies lonafarnib as respiratory syncytial virus fusion protein inhibitor. *Nat. Commun.* **15**, 1173 (2024).
24. Fang, X.-D. et al. Host casein kinase 1-mediated phosphorylation modulates phase separation of a rhabdovirus phosphoprotein and virus infection. *ELife* **11**, e74884 (2022).
25. Liang, Y. et al. Actomyosin-driven motility and coalescence of phase-separated viral inclusion bodies are required for efficient replication of a plant rhabdovirus. *New. Phytol.* **240**, 1990–2006 (2023).
26. Lin, W. & Nagy, P. D. Co-opted cytosolic proteins form condensate substructures within membranous replication organelles of a positive-strand RNA virus. *New. Phytol.* **243**, 1917–1935 (2024).
27. Liang, Q. et al. MolPhase, an advanced prediction algorithm for protein phase separation. *EMBO J.* **43**, 1898–1918 (2024).
28. Plant virology in the 21st century in China: Recent advances and future directions. *J. Integr. Plant Biol.* **66**, 579–622 (2024).
29. Zan, N. N., Li, J., He, H. F., Hu, D. Y. & Song, B. A. Discovery of novel chromone derivatives as potential anti-TSWV agents. *J. Agric. Food Chem.* **69**, 10819–10829 (2021).
30. Oiver, J. E. & Whitfield, A. E. The genus tospovirus: Emerging bunyaviruses that threaten food security. *Ann. Rev. Virol.* **3**, 101–124 (2016).
31. Hong, H. et al. Antiviral RISC mainly targets viral mRNA but not genomic RNA of tospovirus. *PLoS Pathog.* **17**, e1009757 (2021).
32. Olschewski, S., Cusack, S. & Rosenthal, M. The cap-snatching mechanism of bunyaviruses. *Trends Microbiol.* **28**, 293–303 (2020).
33. Ma, X., Zhou, Y. & Moffett, P. Alterations in cellular RNA decapping dynamics affect tomato spotted wilt virus cap snatching and infection in Arabidopsis. *New. Phytol.* **224**, 789–803 (2019).
34. Xu, M. et al. Bunyaviral N proteins localize at RNA processing bodies and stress granules: the enigma of cytoplasmic sources of capped RNA for cap snatching. *Viruses* **14**, 1679 (2022).
35. Feng, Z. K., Chen, X. J., Bao, Y. Q., Dong, J. H., Zhang, Z. K. & Tao, X. R. Nucleocapsid of Tomato spotted wilt tospovirus forms mobile particles that traffic on an actin / endoplasmic reticulum network driven by myosin XI-K. *New. Phytol.* **200**, 1212–1224 (2013).
36. Gaspar, A., João Matos, M., Garrido, J., Uriarte, E. & Borges, F. Chromone: A valid scaffold in medicinal chemistry. *Chem. Rev.* **114**, 4960–4992 (2014).
37. Xu, H. et al. Bioactive compounds from Huashi Baidu decoction possess both antiviral and anti-inflammatory effects against COVID-19. *Proc. Natl. Acad. Sci. USA* **120**, e2301775120 (2023).
38. Dinda, B., Dinda, M., Dinda, S. & De, U. C. An overview of anti-SARS-CoV-2 and anti-inflammatory potential of baicalein and its metabolite baicalin: Insights into molecular mechanisms. *Eur. J. Med. Chem.* **258**, 115629 (2023).
39. Han, Y. et al. Design, synthesis, and antiviral activity of novel rutin derivatives containing 1,4-pentadien-3-one moiety. *Eur. J. Med. Chem.* **92**, 732–737 (2015).
40. Shinde, S. D., Sakla, A. P. & Shankaraiah, N. An insight into medicinal attributes of dithiocarbamates: Bird's eye view. *Bioorg. Chem.* **105**, 104346 (2020).
41. Sağlık, B. N. et al. Synthesis, characterization and carbonic anhydrase I and II inhibitory evaluation of new sulfonamide derivatives bearing dithiocarbamate. *Eur. J. Med. Chem.* **198**, 112392 (2020).
42. Zhang, M., He, Y. & Wei, M. Design, synthesis and biological evaluation of matrine-dithiocarbamate hybrids as potential anticancer agents. *Eur. J. Med. Chem.* **254**, 115375 (2023).
43. Brier, L. et al. Novel dithiocarbamates selectively inhibit 3CL protease of SARS-CoV-2 and other coronaviruses. *Eur. J. Med. Chem.* **250**, 115186 (2023).
44. Salata, C., Calistri, A., Parolin, C., Baritussio, A. & Palù, G. Antiviral activity of cationic amphiphilic drugs. *Expert Rev. Anti-Infect. Ther.* **15**, 483–492 (2017).
45. Kitagawa, T., Matsumoto, A., Terashima, I. & Uesono, Y. Antimalarial quin-acrine and chloroquine lose their activity by decreasing cationic amphiphilic structure with a slight decrease in pH. *J. Med. Chem.* **64**, 0c02056 (2021).
46. Jack, A. et al. SARS-CoV-2 nucleocapsid protein forms condensates with viral genomic RNA. *PLoS Biol.* **19**, e3001425 (2021).
47. Zhao, D. et al. Understanding the phase separation characteristics of nucleocapsid protein provides a new therapeutic opportunity against SARS-CoV-2. *Protein Cell* **12**, 734–740 (2021).
48. Huang, Y. et al. Methylene blue accelerates liquid-to-gel transition of tau condensates impacting tau function and pathology. *Nat. Commun.* **14**, 5444 (2023).
49. Quek, R. T. et al. Screen for modulation of nucleocapsid protein condensation identifies small molecules with anti-coronavirus activity. *ACS Chem. Biol.* **18**, 583–594 (2023).
50. Wang, Y. et al. Dissolution of oncofusion transcription factor condensates for cancer therapy. *Nat. Chem. Biol.* **19**, 1223–1234 (2023).
51. Franzmann, M. T. et al. Phase separation of a yeast prion protein promotes cellular fitness. *Science* **359**, eaao5654 (2018).
52. Fujioka, Y. et al. Phase separation organizes the site of autophagosome formation. *Nature* **578**, 301–305 (2020).
53. Ray, S. et al.  $\alpha$ -Synuclein aggregation nucleates through liquid-liquid phase separation. *Nat. Chem.* **12**, 705–716 (2020).
54. King, M. R. et al. Macromolecular condensation organizes nucleolar sub-phases to set up a pH gradient. *Cell* **187**, 1889–1906 (2024).
55. Feng, M. F. et al. Rescue of tomato spotted wilt virus entirely from complementary DNA clones. *Proc. Natl. Acad. Sci. USA* **117**, 1181–1190 (2020).
56. Liu, Y. et al. First Report on Anti-TSWV Activities of Quinazolinone Derivatives Containing a Dithioacetal Moiety. *J. Agric. Food Chem.* **69**, 12135–12142 (2021).
57. Li, J., Zan, N., He, H., Hu, D. & Song, B. Piperazine derivatives containing the  $\alpha$ -ketoamide moiety discovered as potential anti-tomato spotted wilt virus agents. *J. Agric. Food Chem.* **71**, 6301–6313 (2023).
58. He, S. et al. Linker histone H1 drives heterochromatin condensation via phase separation in Arabidopsis. *Plant Cell* **36**, 1829–1843 (2024).
59. Cui, S. et al. The RNA binding protein EHD6 recruits the m6A reader YTH07 and sequesters OsCOL4 mRNA into phase-separated ribonucleoprotein condensates to promote rice flowering. *Mol. Plant* **17**, 935–954 (2024).
60. Guo, Y. et al. Distinct mechanism for the formation of the ribonucleoprotein complex of tomato spotted wilt virus. *J. Virol.* **91**, e00892-17 (2017).
61. Komoda, K., Narita, M., Yamashita, K., Tanaka, I. & Yao, M. The asymmetric trimeric ring structure of the nucleocapsid protein of tospovirus. *J. Virol.* **91**, e01002-17 (2017).
62. Garcia-Jove Navarro, M. et al. RNA is a critical element for the sizing and the composition of phase-separated RNA-protein condensates. *Nat. Commun.* **10**, 3230 (2019).

63. Sanders, D. W. et al. Competing protein-RNA interaction networks control multiphase intracellular organization. *Cell* **181**, 306–324 (2020).
64. Guillén-Boixet, J. et al. RNA-induced conformational switching and clustering of G3BP drive stress granule assembly by condensation. *Cell* **181**, 346–361 (2020).
65. Roden, C. & Gladfelter, A. S. RNA contributions to the form and function of biomolecular condensates. *Nat. Rev. Mol. Cell Biol.* **22**, 183–195 (2021).
66. Wadsworth, G. M. et al. RNA-driven phase transitions in biomolecular condensates. *Mol. Cell* **84**, 3692–3705 (2024).
67. Li, J. et al. Structure and function analysis of nucleocapsid protein of tomato spotted wilt virus interacting with RNA using homology modeling. *J. Biol. Chem.* **290**, 3950–3961 (2015).
68. Song, W. et al. Substrate-induced condensation activates plant TIR domain proteins. *Nature* **627**, 847–853 (2024).
69. Bose, M., Lampe, M., Mahamid, J. & Ephrussi, A. Liquid-to-solid phase transition of oskar ribonucleoprotein granules is essential for their function in Drosophila embryonic development. *Cell* **185**, 1308–1324 (2022).
70. Visser, B. S. et al. The role of biomolecular condensates in protein aggregation. *Nat. Rev. Chem.* **8**, 686–700 (2024).
71. Jin, J. et al. Recent achievements in antiviral agent development for plant protection. *J. Agric. Food Chem.* **71**, 1291–1309 (2023).
72. Wang, Y., Luo, Y., Hu, D. & Song, B. Design, Synthesis, Anti-tomato spotted wilt virus activity, and mechanism of action of thienopyrimidine-containing dithioacetal derivatives. *J. Agric. Food Chem.* **70**, 6015–6025 (2022).
73. Zhong, F. et al. Eco-friendly cinnamic acid derivatives containing glycoside scaffolds as potential antiviral agents. *J. Agric. Food Chem.* **71**, 17752–17762 (2023).
74. Liang, T., Dong, Y. & Cheng, I. et al. In situ formation of biomolecular condensates as intracellular drug reservoirs for augmenting chemotherapy. *Nat. Biomed. Eng.* **8**, 1469–1482 (2024).
75. Leppert, A. et al. Controlling drug partitioning in individual protein condensates through laser-induced microscale phase transitions. *J. Am. Chem. Soc.* **146**, 19555–19565 (2024).
76. Ambadi Thody, S. et al. Small-molecule properties define partitioning into biomolecular condensates. *Nat. Chem.* **16**, 1794–1802 (2024).
77. Dai, Y. et al. Biomolecular condensates regulate cellular electrochemical equilibria. *Cell* **187**, 5951–5966 (2024).
78. Liu, Y. et al. Proteolysis in plant immunity. *Plant Cell* **36**, 3099–3115 (2024).
79. Qin, M. et al. LATS2 condensates organize signalosomes for Hippo pathway signal transduction. *Nat. Chem. Biol.* **20**, 710–720 (2024).
80. Wells, J. A. & Kumru, K. Extracellular targeted protein degradation: an emerging modality for drug discovery. *Nat. Rev. Drug Discov.* **23**, 126–140 (2024).
81. Chen, Y., Liu, F., Pal, S. & Hu, Q. Proteolysis-targeting drug delivery system (ProDDS): integrating targeted protein degradation concepts into formulation design. *Chem. Soc. Rev.* **53**, 9582–9608 (2024).
82. Shi, Y. et al. BRD4-targeting PROTAC as a unique tool to study biomolecular condensates. *Cell Discov.* **9**, 47 (2023).
83. Jia, W., Li, W., Li, Z. & Li, P. An all-in-one targeted protein degradation platform guided by degradation condensates-bridging bi-specific nanobodies. *Cell Res.* **34**, 389–392 (2024).
84. Lu, P. & Cheng, Y. et al. Selective degradation of multimeric proteins by TRIM21-based molecular glue and PROTAC degraders. *Cell* **187**, 7126–7142 (2024).
85. May, J. P. Plant viruses and biomolecular condensates: novel perspectives in virus replication strategies. *New. Phytol.* **243**, 1636–1638 (2024).

## Acknowledgements

The authors acknowledge financial support from the National Natural Science Foundation of China (No. 32302388 to R.S. and No. 32330087 to B.S.). The authors thank Dr. Mingfeng Feng and Prof. Dr. Xiaorong Tao (College of Plant Protection, Nanjing Agricultural University, China) for assistance in the plasmid construction.

## Author contributions

N.Z. conducted most of the experiments. J.L., S.W., J.Z.L., and F.C. contributed to some experiments. J.Y. created the pattern diagram. R.S. and B.S. conceptualized and directed the project and drafted the manuscript with assistance from all co-authors. All authors contributed to part of the experiments and/or discussions.

## Competing interests

The authors declare no competing interests.

## Additional information

**Supplementary information** The online version contains supplementary material available at <https://doi.org/10.1038/s41467-025-57281-z>.

**Correspondence** and requests for materials should be addressed to Baoan Song or Runjiang Song.

**Peer review information** *Nature Communications* thanks Jared May and the other anonymous reviewer(s) for their contribution to the peer review of this work. A peer review file is available.

**Reprints and permissions information** is available at <http://www.nature.com/reprints>

**Publisher's note** Springer Nature remains neutral with regard to jurisdictional claims in published maps and institutional affiliations.

**Open Access** This article is licensed under a Creative Commons Attribution-NonCommercial-NoDerivatives 4.0 International License, which permits any non-commercial use, sharing, distribution and reproduction in any medium or format, as long as you give appropriate credit to the original author(s) and the source, provide a link to the Creative Commons licence, and indicate if you modified the licensed material. You do not have permission under this licence to share adapted material derived from this article or parts of it. The images or other third party material in this article are included in the article's Creative Commons licence, unless indicated otherwise in a credit line to the material. If material is not included in the article's Creative Commons licence and your intended use is not permitted by statutory regulation or exceeds the permitted use, you will need to obtain permission directly from the copyright holder. To view a copy of this licence, visit <http://creativecommons.org/licenses/by-nc-nd/4.0/>.

© The Author(s) 2025